

POLITECNICO DI TORINO

Department of Mechanical and Aerospace Engineering



**Politecnico
di Torino**



European Space Agency

ISL-BASED SYSTEM FOR GNSS EVOLUTION

MASTER THESIS

Candidate:
Anna MAURO
ID: 290618

Supervisor:
Prof. Roberto GARELLO

Tutor:
Dr. Riccardo DELLAGO

M.Sc in Aerospace Engineering
A.Y. 2022-2023

Copyright © October 2023 by Anna Mauro
All rights reserved.

This content is original, written by the Author, Anna Mauro. All the non-originals information, taken from previous works, are specified and recorded in the Bibliography.

When referring to this work, full bibliographic details must be given, i.e. Anna Mauro, "*Thesis Title*". 2023, Politecnico di Torino, Master in Aerospace Engineering, Supervisors: Roberto Garelo, Riccardo Dellago.

Printed in Italy

"It is the time you have wasted for your rose, that makes your rose so
important."

ANTOINE DE SAINT-EXUPÉRY

Abstract

The purpose of this thesis is to conduct a feasibility study of the future potential architecture designed to implement Laser Communication Terminals (LCTs) into future generations of Galileo satellites. The study takes into consideration a range of technological trade-offs with the necessary adaptations of the satellite platform. The study then outlines two distinct concepts: a first concept of optical communication only and a second concept with a hybrid communication system, using both radio frequencies and optical terminals. Finally, a concept for the transition system to the new technology is also defined, envisioning a future final system that is implemented over time. The performance is then analyzed and compared against the requirements dictated by various mission case studies, both present and future taking into account the new capabilities brought by optical links.

Sommario

Lo scopo di questa tesi è uno studio di fattibilità di un'architettura che prevede l'implementazione di Laser Communication Terminal (LCT) a bordo di future generazioni di satelliti Galileo, considerando alcuni trade-off tecnologici e l'adattamento della piattaforma del satellite. Vengono definiti un concept con sola comunicazione ottica ed un secondo concept con un sistema di comunicazione ibrido, che utilizza sia radiofrequenze che terminal ottici. Viene poi definito anche un concept di sistema di transizione alla nuova tecnologia, immaginando un futuro sistema finale che viene implementato nel tempo. Infine, verranno analizzate le performance e confrontate con i requisiti dettati dai diversi casi studio di missione, presenti e futuri.

Acknowledgements

First of all, I have to express my deepest, most sincere gratitude to my tutor and supervisor Riccardo for giving me the chance to work on an extremely interesting topic and supporting me with patience and advice during the whole six months. I also have to thank Christina, Mathew and the big team in the Galileo Program Department at ESA ESTEC for taking an interest in my work and supporting me with advice and stimulating talks.

To be continued...

Table of Contents

Abstract	I
Sommario	II
Acknowledgements	III
List of Figures	VI
List of Tables	VIII
1 Introduction	1
1.1 Thesis outline	1
2 Intersatellite links in GNSS constellations	2
2.1 History of Intersatellite Links	2
2.2 Current Status of GNSS ISL	4
2.3 The case for ISLs in Navigation Constellations	5
2.4 ISL in Galileo	5
3 Optical Terminals for inter-satellite communications	6
3.1 Carrier Characteristics	7
3.2 Types of Lasers	8
3.3 Optical Transceiver Components	9
3.4 Modulation Schemes	10
3.4.1 BPSK and M-PPM	11
3.4.2 Coding	12
3.5 Aperture Diameter	12
3.6 Counter-rotation of the terminal	15
3.7 Acquisition, Tracking and Pointing	15
3.7.1 ATP schemes	16
3.7.2 Pointing error budget	18
3.8 Receiver	22
3.8.1 Choice of Detection method	22

3.8.2	Detectors	23
3.8.3	Required Received Power	23
3.9	Operating Wavelength	24
3.10	Point-ahead-angle and Doppler Shift	25
3.11	Link Budget	26
4	Network Architecture	31
4.1	Inter-satellite link planning	31
4.2	OISL system	35
4.2.1	Contacts structure	36
4.2.2	ID Association	36
4.2.3	Timeslot structure	37
4.2.4	Connectivity Matrix	41
4.3	Hybrid RF and Optical system	42
4.4	Operational Use Cases	45
4.5	Transition System	48
5	New Use Cases for GNSS	49
5.1	Towards routine contacts with ISL	49
5.2	European Data Relay System	50
5.3	Ground - Space Optical Links	51
5.4	ODTS	52
5.5	Novel architectures for GNSS	53
6	Conclusions and further developments	55
	References	56

List of Figures

2	Electromagnetic spectrum	3
3	Components of a full-duplex Laser Communication Terminal (LCT) . .	6
4	Optical laser unit, from TESAT for the EDRS relay satellite	7
5	Diagram of the optical antenna of a laser communication terminal . . .	13
6	Beam Diameter vs link distance, with $D_T = 10$ cm	13
7	Amount of Power Received at the maximum distance, for different beam waists	14
8	Pointing error vs beam waist	14
9	Capabilities and major features of ATP mechanisms	16
10	Uncertainty Cone	17
11	Continuous Spiral scan pattern	18
12	Pointing scene	19
13	Contributions to the pointing error	21
14	Doppler shift between Satellite ID1 and other satellites from different orbital planes	26
16	Beam diameter vs Link Distance	28
17	Power received versus optical power in output from the transmitter . .	29
18	Galileo FOC constellation	32
19	In green, permanently available links.	34
20	A few connectivity configurations, which alternating in time connect all satellites	34
22	Timeslot structure for a ring scheme from satellite A to satellite E . . .	37
24	Example of a Contact Plan over time	39
23	Minimum dissemination time, in the case of a ring configuration scheme and maximum number of hops	39
25	Example of a Connectivity Matrix	42
26	Possible network topologies for a hybrid network architecture, and view of the different links coexisting in the constellation	44

27	Example for a dissemination path with 3 Gateways, each communicating with two operative payloads. This representation in normalized 3-D space was used to take into account more information than was obtainable in a MATLAB Satellite Scenario, and represents the gateway satellites in red, and their separate "rings" or "branches" in three different colors	47
29	Time necessary for dissemination vs Data Rate, for different number of gateways connected to ground	49
30	Time necessary for dissemination vs Data Rate, zoom on 4-hour limit	50
31	Initial Optical Nucleus Network	52

List of Tables

1	Modulation Schemes and their respective missions	10
2	Theoretical sensitivity of different coherent receivers	11
3	Sensitivity (minimum power required) for direct detection	24
4	Sensitivity (minimum power required) for coherent detection	24
5	Link budgets	30
6	Orbital Parameters	32
7	Latency Budget for Single Hop	40
8	Latency Budget for Open Ring	41

CHAPTER *1*

Introduction

GNSS systems are incorporating more and more satellite connected architectures and networks to better fulfil their mission, and this has been happening through the increasing use of Intersatellite Links. ISLs can provide improvements not only in position accuracy at user level and mission products dissemination, but also in terms of constellation management. For this to become a reality, ISL requires not only technological development but also advanced and robust network architectures, protocols and planning techniques that need to consider the specific conditions and use cases to be covered. The main function of Inter-Satellite Links is to accurately measure the distance and clock corrections between satellites and to allow communication between satellites, thus improving, in theory, the performance of the GNSS service. OISLs are attractive solutions in terms of size, mass and power while providing multi-Gbps data rate capabilities and a better ranging resolution.

1.1 Thesis outline

The different chapters of this thesis are organised sequentially as follows:

- **Chapter 2:** Inter-satellite links in GNSS constellations
- **Chapter 3:** Optical Terminals for ISL communications
- **Chapter 4:** Network Architectures
- **Chapter 5:** New Use Cases
- **Chapter 6:** Conclusions and further developments

CHAPTER 2

Intersatellite links in GNSS constellations

2.1 History of Intersatellite Links

Currently, both radio frequency and optical intersatellite links are present within space systems. Early ISLs operated on lower frequencies such as VHF, which are no longer adopted in GNSS systems due to their constrained data rate and antenna size limitations. The 1960s was the time when the development for laser communications in space development began, with the purpose of enabling very high data rate applications. Due to the higher frequencies used in laser communication, as can be seen in Fig.2, the amount of bandwidth available for communicating is much larger compared to RF, enabling notably higher data rates. The use of shorter wavelengths also leads to much smaller diameter of the optical antenna and a narrower communication beam divergence. Compared to RF systems with similar performance, the size, weight and power (SWaP) parameter of the laser terminals is typically lower. Laser communications also offer enhanced security as they are very challenging to intercept or to jam, and suffer very little from interference thanks to the narrow beamwidth. Furthermore, presently optical frequencies are unregulated, unlike RF systems that require a licensing process. These are some of the advantages that make optical communication an attractive choice for space systems. It's important to note that laser communications do come with their limitations, and there are situations where radio frequency (RF) communications outperform their optical counterpart. For instance, the small beam divergence can lead to more substantial pointing errors, which would inevitably be more significant. In broadcast applications, RF systems can cover a much larger angular area, while optical systems are generally limited to point-to-point communication. RF transmission currently remains indispensable for ground-to-space communications, primarily due to atmospheric attenuation. This phenomenon makes communication impossible when cloud cover is present, and urge the ground segment to establish its

risk at acceptable levels.

2.2 Current Status of GNSS ISL

Before being applied in navigation constellation systems, intersatellite links (ISLs) found application in communication constellations, relay satellites, and satellite formation flights. Between 1983 and 2002, the United States launched its Tracking and Data Relay Satellites (TDRS) equipped with S and Ku frequency bands, later enhanced with the additional Ka-band capability bringing reception rates up to 800 Mbps. The American Iridium satellite constellation, consisting of 66 satellites, is the only large constellation in the world that employs ISLs in the Ka-band. This is accomplished through phased array antennas with maximum transmission rate of 25 Mbps in half-duplex mode.

A navigation constellation requires updated inter-satellite ranging measurements in support of the orbit determination process while simultaneously using the same network to upload and download data from the constellation, other constellation systems usually feature a less complex system with fewer inter-satellite links, no network concept, simpler inter-satellite routing and less demanding antenna rotations. In GNSS systems, the Ground Segment routinely gathers observation data from the satellites, crucial for orbit calculation, orbit determination, and ephemeris updates. The inter-satellite link serves as a bridge for collecting data from satellites not directly linked to the ground stations. Through this development, the ground operation management is simplified and the autonomy of the constellation can be improved [2] [3] [4] [5] [6].

GPS is the first GNSS system with ISLs, where it was proposed to support autonomous satellite navigation. Starting from the Block IIR, the GPS satellites have been equipped with ISL transceivers (in the UHF band) realizing autonomous navigation functions, inter-satellite communication and ranging [7]. By on-board processing of the inter-satellite measurements, the satellite ephemeris and clock correction parameters are autonomously generated. In GPS III, the brand-new design will feature high-speed transmission and directional inter-satellite links with the introduction in the GPS III B of the V-band link [8].

Russia's GLONASS began to implement the S-band ISL with GLONASS-K, to improve the orbit determination accuracy and autonomous navigation ability of satellites. In addition, successive satellites also carry two payloads for OISLs, mainly used for time synchronization and the transmission of a small amount of data.

The ISLs within BDS-3, based on Ka-band phased array antennas, form a complex intersatellite network with high performance requirements across various aspects such

as antenna pointing control, network topology and protocol, and ISR accuracy. Currently, the BeiDou GNSS system is the most advanced system using ISLs [9].

2.3 The case for ISLs in Navigation Constellations

The basic use cases enabled by the use of inter-satellite links are:

- **Precise ODTS:** Inter-satellite links in navigation satellite systems create a dynamic wireless network that enables precise measurements and data transmission between the satellites. Modern satellite navigation depends on broadcasting synchronized navigation signals from a Medium Earth Orbit (MEO) constellation. ODTS represents a central process in the architecture of GNSS systems. Traditional GNSS systems aim at eliminating time by computing differences between receivers and/or satellites to estimate the satellites' orbits, which then become the basis for determining time offsets.
- **Data communication:** Utilizing inter-satellite links enhances the TT&C capabilities and extends data communication coverage, ensuring virtually uninterrupted monitoring and efficient management of the constellation. Additionally, this facilitates detection and management of anomalies and failures, meeting the demands for real-time monitoring and control.

2.4 ISL in Galileo

Currently, the European Galileo first generation of satellites does not utilize intersatellite links (ISLs), relying mainly on distributed ground monitoring stations for orbit determination. However, the next generation of Galileo will incorporate their use for both ranging and communication functions, to routinely cross-check the satellites' performance and reduce their dependency on ground availability [10]. However, due to the limitation of on-board computing capability, an excessively complex dynamic model cannot be adopted. As future iterations of the Galileo system or other GNSS systems are developed, the inclusion of optical intersatellite links could be considered as a means to enhance performance and capabilities.

CHAPTER 3

Optical Terminals for inter-satellite communications

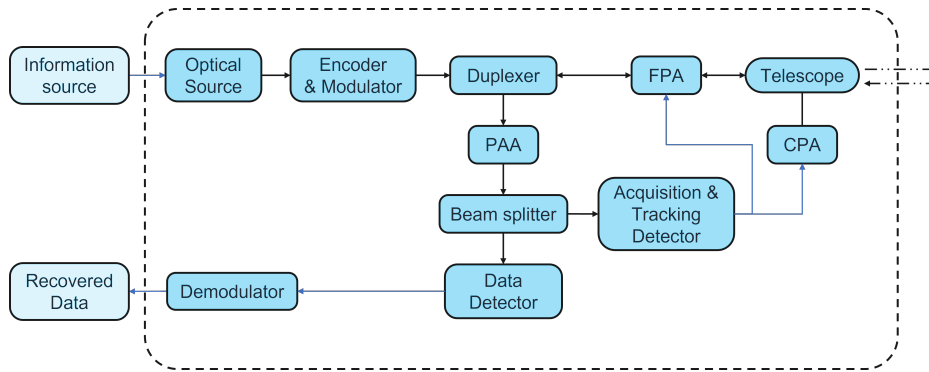


Figure 3: Components of a full-duplex Laser Communication Terminal (LCT)

The basic components of an optical communication system are shown in Fig. 3. It consists of the optical power source, modulator and encoder, ATP system, filter for background suppression (not shown in the figure), optical transmitting and receiving aperture and detector, demodulator and decoder at the receiving end. The Optical Source is a laser, preferably operating in a single transverse mode so as to achieve the highest possible antenna gain. An external modulator is usually used to impress the data signal onto the beam. The modulated and encoded beam then passes through an optical duplexer and a Fine Pointing Assembly before it enters the optical antenna, the telescope. The received radiation is also collected by the telescope (or also commonly, a different telescope) and the fine pointing assembly, and with the aid of a duplexer is directed to the receiving part of the terminal. With a beam splitter, part of the optical components in the terminal, one part of the beam is directed onto the Data Detector for demodulation and the other part is used for controlling the Fine and Coarse pointing mechanisms (in a way such that the alignment is kept between transmitting and

receiving terminals). A Point-Ahead Assembly has to be inserted in either the transmit or receive path to allow electronic control of the alignment between transmission and reception terminals. The relative position of the different spacecraft subsystems is also dependent on admissible vibration levels reaching the laser terminal.

Before transmitting data a beacon signal is transmitted from one satellite to the other, either with the same communication beam or a separate beacon. During acquisition, performed by the ATP system, one satellite interrogates the Uncertainty Area (or Uncertainty Cone) of the target satellite by scanning of the area with the transmitting beam. Once the target satellite detects and acquires the beacon, there can be the transition from acquisition to tracking: once the link has been acquired and connection is established, data communication can start.

Fig.4 shows the Tesat LCT for geostationary applications, used onboard Alphasat, as

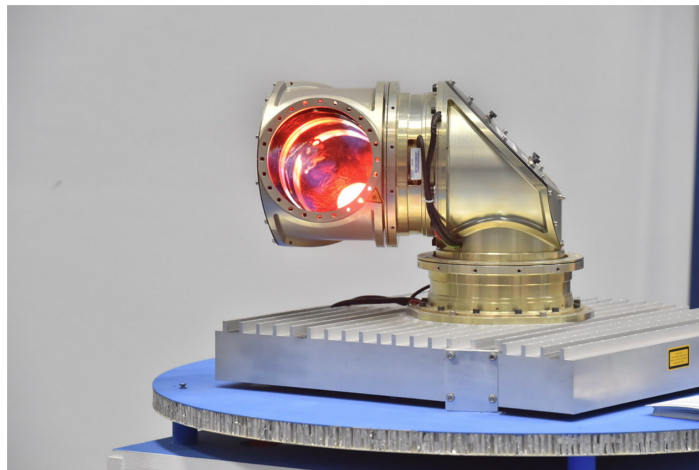


Figure 4: Optical laser unit, from TESAT for the EDRS relay satellite

well as on the EDRS satellites, and supports optical links between LEO and geostationary satellites. In the design of the OISL link with initial given requirements, some trade-offs have to be made among various design parameters for both the transmitter and the receiver, which will be discussed in the following sections.

3.1 Carrier Characteristics

The electromagnetic waves travelling through space can be described with frequency ν that travels at the speed of light c , related by the carrier wavelength $c = \lambda\nu$ and with energy given by . Figure 2 brings a sense of the broad range of wavelengths

and frequencies that can be used for communication. The carrier characteristics have different impacts on the transceiver design: for example, the size of the antenna and the effect of diffraction in space are proportional to the carrier wavelength, while frequency is proportional to available bandwidth. Beam divergence angle for a Gaussian beam is given by

$$\theta = \lambda/D_{Tx} \tag{1}$$

where D_{Tx} is the transmitter aperture diameter.

This highlights the key difference between high-rate RF and FSO communication: while FSO is able to use bandwidth as a flexible design parameter, RF communication needs to be spectrally efficient to use high data rates, albeit sacrificing energy efficiency. Energy-per-photon is given by Planck's relation: $E = h\nu = hc/\lambda$, and it is proportional to the shot noise of the transmitted signal, and therefore impacts the receiver sensitivity. As E increases for a given power, the shot noise of the signal increases due to the lower number of photons in the signal. This drives high-sensitivity receiver design.

3.2 Types of Lasers

The most important component of the transmitter is, clearly, the laser working as an optical source for the communication subsystem. Mostly, advances for these applications have been made in semiconductor diode lasers and solid-state lasers, for their high efficiency, long operative life, high power, high beam quality, and compact sizes and volumes. Solid-state lasers for communications which among the available options generates the most power most efficiently. These lasers are pumped by light from laser diodes, and can be considered as devices that absorb incoherent laser light from laser diodes and emit coherent light with high spectral purity. The DPSSL (Diode-Pumped Solid-State Laser) has demonstrated its suitability for coherent homodyne optical communication in the EDRS terminals, which have been operating in orbit for several years.

Solid-state lasers became the choice for free-space optical communication applications, the most common being the Nd/YAG whose laser wavelength is 1064 nm. Semiconductor lasers are also convenient for their compact size and light weight, but have low output power, and therefore require additional amplification for long distance communication. They also get damaged easily, and usually require an alternate or redundant laser source for reliability issues.

3.3 Optical Transceiver Components

- **Light source:** Optical sources lie in the wavelength range from 700 nm to 10,000 nm. The most widely used for beacon and data transmitting signals, however, are 1064 nm and 1550 nm. Both 1064 nm and 1550 nm light sources are going to be considered in this study, in order to conduct a trade-off between the two operating wavelengths. As we will see, this is a fundamental choice in the design phase as it has an influence on many aspects of the link.
- **Modulator:** Optical satellite communication terminals are capable of supporting various binary and multi-level modulation formats. To correct transmission errors, error correcting codes are implemented simultaneously with modulation. Both modulation and encoding for wireless optical communications are advanced and mature technologies [11], and some guidelines can already be found in the various standards that are appearing for space optical communication terminals [12], [13].
- **Local Oscillator:** In the case of coherent detection, the signal to be detected is superposed to the beam of the LO running on the same frequency as the signal's carrier. The optical phases of both, signal and local oscillator need to be locked by a control loop. The two light waves are involved in a mixing process, and they are then both received by the photodetector. The optical output power of the LO can usually be smaller, and it may be chosen with a wider tuning range, to compensate for frequency uncertainties and for the entire Doppler shift between the moving satellites. In most systems, such compensation is achieved solely by tuning the LO laser [11].
- **Optical Antenna:** The optical antenna is essentially a telescope which enlarges the beam's diameter, reducing its divergence to obtain a narrow, high-gain laser beam. On the receiving path, the telescope collects and concentrates the incoming radiation.
- **Detector and filter:** The photodetector, which is at the heart of any optical receiver, is usually a semiconductor photodiode. Coherent communication systems use the most sensitive receivers, and have the lowest vulnerability to stray light or background light. The filter bandwidth should be sufficiently wide to pass the information signal without any alteration and to account for Doppler shift between the moving satellites, but should not be too wide because it will bring to an increase in background noise contribution.

- **Point Ahead Assembly:** After being collimated, the laser beam falls on the point ahead assembly, which has to be inserted in the optical path to generate an offset angle between the transmitted and received signals to compensate for the running time of the laser light towards the receiving end.
- **ATP system:** the key components are the CPA, which is used to control the pointing of the laser beam towards the target, and the FPA, typically implemented with fast steering mirrors (FSM) for very precise and fast beam steering.
- **Optical subsystem:** provides the optical chain through which both transmitted and received optical signals are guided; it is typically fiber-based.

3.4 Modulation Schemes

Common data transmission formats for optical communications are on-off keying (OOK), PPM, and PSK; Pulse Position modulation (PPM) allows multiple bits per photon detection and is ideal for photon-starved channels, while BPSK is another high-efficiency code applied together with optically preamplified receivers to high-rate laser communications. In Table 1 are listed the modulation formats currently or formerly used for optical communications in space. On-off keying (OOK) and pulse position modulation

Wavelengths	Modulation schemes	Missions
808 nm	On-Off Keying (OOK) - Non-Return to Zero (NRZ)	SILEX, ARTEMIS, OICETS, LOLA
1064 nm	BPSK - NRZ	TerraSAR-X, NFIRE, ALPHASAT, EDRS
1550 nm	OOK - NRZ, PPM, DPSK	LADEE, OPALS, OPTEL- μ , DSOC

Table 1: Modulation Schemes and their respective missions

(PPM) are called *direct detection methods* since they modulate data on the intensity of light, which is the only signal characteristic to be measured by the receiver. In *coherent detection methods*, the use of the local oscillator (LO), giving extra degrees of freedom

to encode data and fully use channel capacity by enabling to recover information also on phase and polarization of the signal [14]. Homodyne PSK detection currently shows the highest known receiver sensitivity. For an ideal receiver, theoretical performance can be calculated by:

$$BER = \frac{1}{2}e^{-N} \quad (2)$$

Eq. 2 is useful to assess the performance of various receivers in different optical communication systems. Quantum noise, which represents one of the fundamental limits to optical receiver sensitivity, is what is typically referred to as "shot noise" and accounts for the randomness of photon arrival [14]. Theoretical sensitivity is dependent on the modulation type and is often measured in terms of the number of photons-per-bit required to achieve a BER of 10^{-9} . These sensitivities for different types of receivers are:

Detection scheme	IM/DD	Homodyne BPSK	2-PPM
BER	$\frac{1}{2}e^{-\eta N_P}$	$\frac{1}{2} \operatorname{erfc} \sqrt{2\eta N_P}$	$\frac{1}{2}e^{-\frac{\eta N_P}{2}}$
Sensitivity	20 ppb	9 ppb	20 ppb

Table 2: Theoretical sensitivity of different coherent receivers

The required photons/bit, and therefore power at the receiver, is the lowest for Homodyne BPSK modulation and detection method. However, as will be explained in later chapters, there are still reasons to prefer a noncoherent communication system. Although, the most recent recommendations and standards from the CCSDS and SDA recommend using OOK and PPM as modulation formats.

3.4.1 BPSK and M-PPM

BPSK has been used operationally for optical intersatellite links primarily by TESAT for the EDRS nodes, achieving 2 Gbps across 45000 km at bit error rates of 10^{-9} . BPSK has been described as being superior to all other optical modulation schemes being the most sensitive for both communication and tracking, and being immune against direct sunlight, maintaining a communication link even with it being directly in the receiver's field-of-view [15].

However, in the latest standards and recommendations, OOK and PPM modulation

formats have been recommended [13], [16], [12]. In particular, the CCSDS recommends LDPC encoding, PN-spreading and mapping into 2-Pulse Position Modulation (2-PPM) symbols. M-PPM has also been long recognized as a power-efficient format. It sacrifices bandwidth for ensuring receiving sensitivity by using minimum optical power: as M increases, the number of PPB required to achieve the same BER is lower. PPM modulation requires that the laser energy be concentrated in high peak pulses, and the mean power is obtained by averaging the peak power for each M slots in a PPM symbol, also considering the time of laser recharge. PPM is a modulation scheme that can be implemented non-coherently, such that the receiver does not need to track the phase of the carrier. The frame sent into the channel is a sequence of laser pulses, for which a slot without a pulse identifies a '0', while an impulse identifies a '1'. Therefore, the receiver must detect the transmitted optical impulses, and the technology used to do this is not unique, with different implementations leading to different mathematical models.

3.4.2 Coding

Forward error correction is a powerful tool that is often a cost-effective means of significantly improving receiver sensitivity. In the Optical Inter-satellite link standards, both LDPC and Convolutional error correcting codes are suggested. At a BER in the scale of 10^{-9} , a coding gain of 3 dB is obtained with LDPC encoding [17], as recommended by the CCSDS Blue Book [13].

3.5 Aperture Diameter

The optical antenna is used to transmit and receive the signals to and from another source or target. An example is shown in Fig.5: the telescope consists of a primary and a secondary mirror, where the laser pulse is reflected before being sent into space. The operation is in fact equal to the one of a communication parabola, with the difference of using mirrors because of the higher optical frequencies. Characterized by smaller wavelengths and narrow lobes, optical antennas can be much smaller than RF antennas, leading to a system with overall lower weight and costs.

In Fig.6, the aperture diameter is indicated as *beam waist* w_0 . The beam waist is the smallest radius of a laser beam, and for very long distances from the source (distances much greater than its Rayleigh range) it can be approximated as the diameter of the telescope. The diameter of the received laser beam spot is inversely proportional to the beam waist: therefore to reduce the required optical output power, the transmitting diameter should be wider. On the other hand, a wider receiver size will increase both

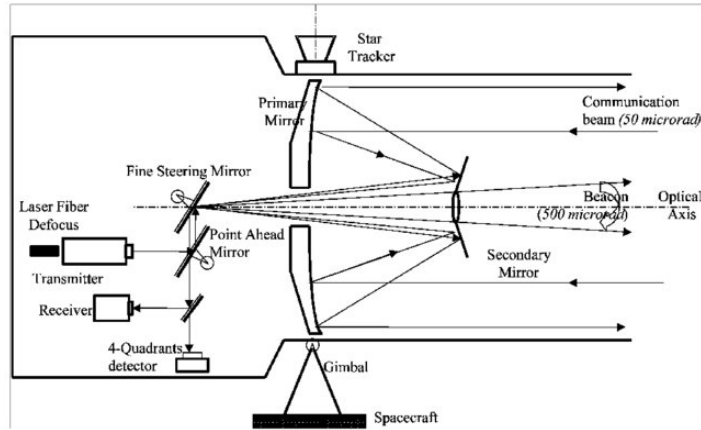


Figure 5: Diagram of the optical antenna of a laser communication terminal

the mass of the terminal and the background noise component, other than requiring a tighter pointing accuracy and a higher sensitivity towards pointing loss. Therefore, it is favourable to keep the diameter size w_0 limited.

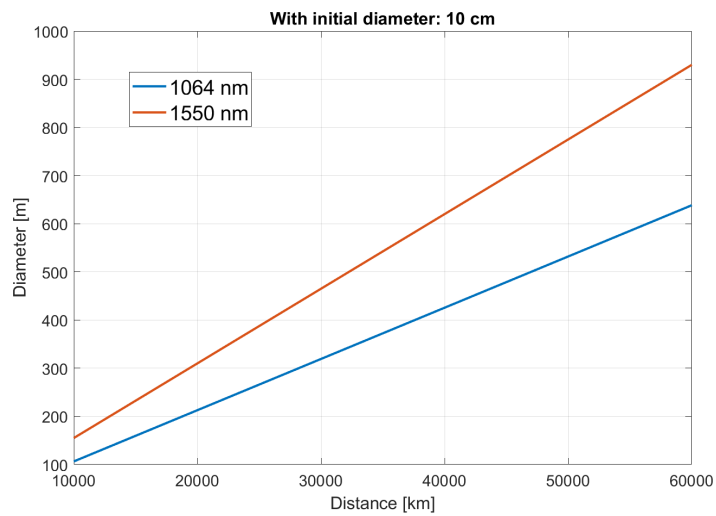


Figure 6: Beam Diameter vs link distance, with $D_T = 10$ cm

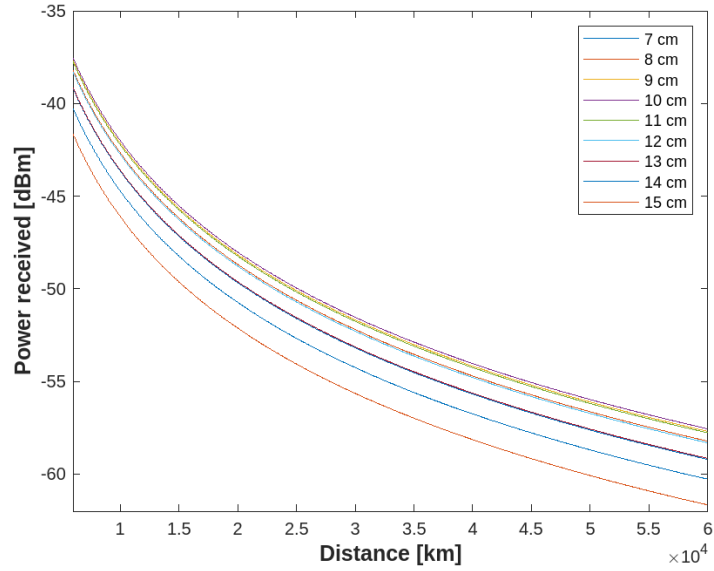


Figure 7: Amount of Power Received at the maximum distance, for different beam waists

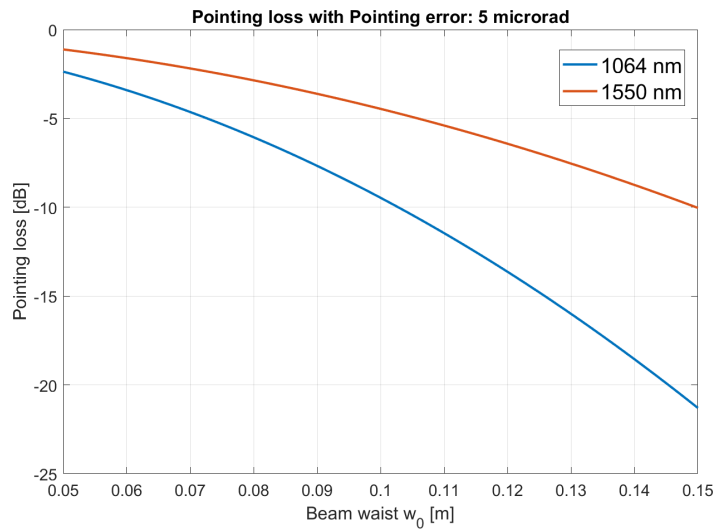


Figure 8: Pointing error vs beam waist

3.6 Counter-rotation of the terminal

The attitude of a navigation satellite is essential for its mission, as it has an impact on the correction of observation errors and the modeling of non-gravitational perturbations. The nominal attitude is determined by two requirements: the navigation signal needs to be received by users on the surface of the Earth, the attitude of the satellite must allow the transmitting antenna to point to the center of the Earth. The second requirement is determined by the orientation of the solar panels perpendicular to the Sun's direction. The "yaw steering guidance" for the Galileo satellites optimizes thermal control for the clocks and the angle between the Sun and the solar panels. The sense of rotation is clockwise (from the satellite looking at Earth), and a Yaw angle of 0 deg corresponds to the in-plane, flight direction (X_{LVLH} in the velocity direction). The roll, pitch and yaw angles are defined with the following axes:

$$\begin{aligned}\vec{Z}_{LVLH} &= -\vec{r} \\ \vec{Y}_{LVLH} &= \frac{-\vec{r} \times \vec{v}}{\|\vec{r} \times \vec{v}\|} \\ \vec{X}_{LVLH} &= -\vec{Y}_{LVLH} \times \vec{Z}_{LVLH}\end{aligned}\tag{3}$$

The Z-axis points towards the Earth's center, the Y-axis is the rotation axis of the solar panels, and the X-axis completes the right-hand coordinate system and points in the satellite's velocity direction. The maximum angular rate for yaw steering, during a 180° turn, is in the order of 0.1°/s. This should also be the maximum angular rate for the counter-rotation of the terminal.

3.7 Acquisition, Tracking and Pointing

The ATP system is the foundation of long-distance spatial optical communication. A simple version of the system can be seen in Fig.3. The key components are the Coarse Pointing Assembly (CPA), which is used to guide and point the laser beam at the receiving target, and the Fine Pointing Assembly (FPA). In addition, most applications require a point-ahead assembly (PAA) to account for the finite light speed and thus the target's angular displacement in order to intercept its trajectory at very long distances. A gimbal allows to rotate in numerous directions, for the wide pointing range required in satellite-to-satellite FSO communication. Due to the vital role of the ATP system in FSO communication, its technology is one of the main factors determining whether the data transmission is successful. In order to achieve reliable communication, it is possible to use a higher power and broader-beam beacon laser and use a closed-loop

tracking system, which can also be identified in Fig.3. From a ranging accuracy point of view, inertial sensors can be used to minimize the impact of such vibrations and jitters.

3.7.1 ATP schemes

ATP mechanisms can be classified according mainly to their mechanics: gimbal-based, mirror-based, gimbal-mirror hybrid, adaptive optics, and others [18]. The ATP systems used in space are inherently more sophisticated than those used in terrestrial applications because of the greater distances to be covered. For inter-satellite links, which usually require a wide angular range of motion, *gimbal-based ATP mechanisms* are usually implemented. These use a mechanical rotary gimbal controlled by motors, and thus are characterized by two or three-axis moving capability of the gimbal, which rotates the terminal to the required azimuth and elevation angles. Gimbals have a relatively coarse pointing resolution (larger step size) than mirror-based ATP mechanisms; the angular pointing resolution of gimbals currently available in the market is in the range of μrad , whereas that of mirror-based ATP mechanisms is in the range of sub- μrad [19]. Therefore a gimbal can be used together with mirror-based mechanisms which use Fast Steering Mirrors (FSMs) to perform beam stabilization, pointing, and tracking. FSMs are lightweight, have high steering speed and fine pointing resolution. The pointing requirements are specified in terms of half-cone Line-Of-Sight (LOS) er-

ATP Mechanism	Pointing Resolution (rad)	Field of Regard	Angular Steering Speed	Mechanics	Dimensionality
Gimbal-based	μrad	Wide	Low	Mechanical	2D
Mirror-based	Sub- μrad	Narrow	High	Mechanical, piezoelectric and electromechanical	2D, 3D
Gimbal-Mirror Hybrid	Sub- μrad	Wide	High	Mechanical, piezoelectric and electromechanical	2D, 3D

Figure 9: Capabilities and major features of ATP mechanisms

rors, or as rotational angle deviations per axes of the pointing reference frame [20]. In order to allow for a beaconless system, the divergence and pointing error of the transmitting beam should allow for fast initial signal acquisition. The satellite's position knowledge has an accuracy of ± 200 m (in all directions), while platform pointing error is in the order of $\theta_u = 1.5$ mrad. The time needed to scan the Field of Uncertainty is to be calculated by the steps needed to cover an area of $\pi\theta_u^2$ using the communication beam. The acquisition process then consists of two steps. There must be an adequate level of received power for an initial reliable acquisition, and when enough

power is received at the target plane, closed-loop tracking can be initiated. The beam divergence is critical to ensure initial detection within the required acquisition time and at the same time allow the transition to the following tracking phase.

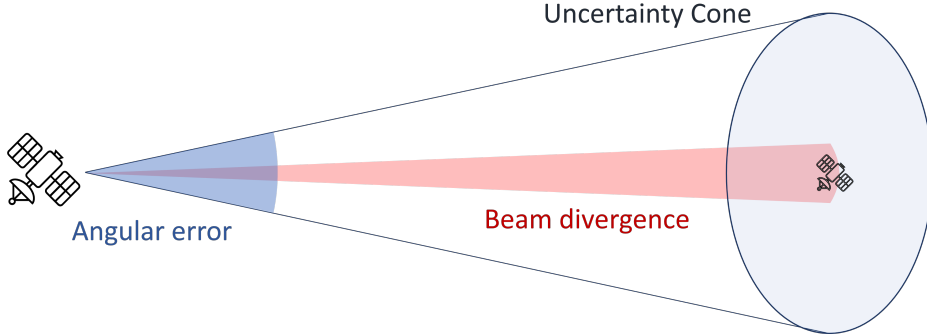


Figure 10: Uncertainty Cone

The Uncertainty Cone is much bigger than the area illuminated by the communication beam: with an attitude control error of $0.1^\circ = 1.5 \text{ mrad}$, its diameter is ~ 88 times bigger than the beam's diameter. Therefore, if no beacon is used, the narrow communication beam is moved within the UC until the signal reaches the receiver. The two methods are named *spatial acquisition with beacon* and *beaconless spatial acquisition*. If using a beacon, pixel sensors are typically used. Mechanical co-alignment must be guaranteed over a wide range of operating temperatures, and this requires a trade off against performance to keep the extra weight low. In beaconless systems, quadrant photodiodes (QPDs) are used as receivers both for acquisition and communication, with the advantage of reduced power and mass as well as higher reliability, due to the QPDs' superior FIT rates. However, this choice places complexity on the algorithm rather than on the hardware for signal acquisition [21].

The spiral scan is the most efficient scanning technique. Moreover, it is the PAT technique described in the most recent CCSDS and SDA Standards for LCTs and OISLs. This type of scan is quite easy to implement, and its trace can be described in polar coordinates as is shown in Fig.11:

$$r_s = \frac{L_\theta}{2\pi} \theta_s \quad (4)$$

In Eq.4, L_θ is the step length related to the beacon beam divergence angle by the relation $L_\theta = \theta_{div}(1 - F_0)$ with overlap factor F_0 a measure of how much each scan spatially overlaps with the previous one. It is clear from these relations that as beam

divergence increases, step length and trace increase, therefore reducing the acquisition time. If beam divergence increases, it also requires higher transmitted power and a larger-sized telescope. In [22] TESAT also refers to the use of spiral scanning tech-

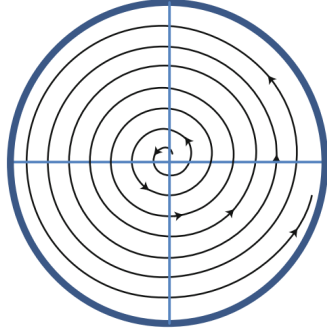


Figure 11: Continuous Spiral scan pattern

nique for beaconless acquisition in similar applications, performed by the point-ahead mechanism of the LCT. The required scan time from the initial point $(0,0)$ to (r_s, θ_s) with dwell time T_{dwell} on each spot can be calculated as:

$$T(r_s) \simeq \frac{\pi \theta_s^2}{L_\theta^2} T_{dwell} \quad (5)$$

$$T_{dwell} = T_R + 2 \frac{R}{c} \quad (6)$$

while the total scan time is given by:

$$T_U(\theta) \simeq \frac{\pi \theta_U^2}{L_\theta^2} T_{dwell} \quad (7)$$

Where one can see the dependence on the size of the UC in θ_U and on the beam's size in L_θ . For the satellite platform, the ratio θ_U/θ_{div} is already around 50-60. It's clear that the communication beam would be too narrow for the link acquisition phase, requiring a beacon signal for fast acquisition.

3.7.2 Pointing error budget

Pointing error is described with respect to the target plane. Translational pointing errors on the target plane are a result of rotational errors about the pointing system

axes. Hence rotational errors about the pointing system x- and y-axis correspond to a displacement error $\epsilon_{x\theta}$ and $\epsilon_{y\Phi}$ on the target plane, respectively. Rotational errors about the z-axis, however, generate rotational errors that can eventually be mapped into x,y displacement errors: if Ψ is the rotation around z:

$$\epsilon = \begin{pmatrix} \epsilon_x \\ \epsilon_y \end{pmatrix} = \mathbf{R}_\Psi(\mathbf{p} + \epsilon_1) - \mathbf{p} \text{ with } \mathbf{p} = \begin{pmatrix} x_p \\ y_p \end{pmatrix} \text{ and } \mathbf{R}_\Psi = \begin{bmatrix} \cos\Psi & -\sin\Psi \\ \sin\Psi & \cos\Psi \end{bmatrix} \quad (8)$$

where the line of sight (LOS) or half-cone error ϵ_1 , assuming radial symmetry, is defined as:

$$\epsilon_1 = \begin{pmatrix} \epsilon_x \\ \epsilon_y \end{pmatrix} \text{ with } |\epsilon_1| = \sqrt{\epsilon_x^2 + \epsilon_y^2} \quad (9)$$

Therefore the resulting pointing error can be described by two translations and one rotation on the target plane.

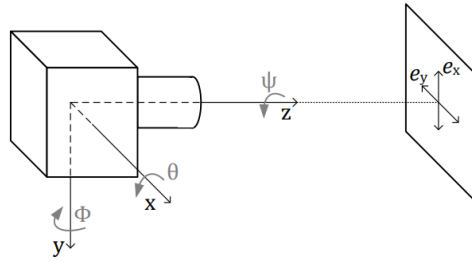


Figure 12: Pointing scene

x, y, z axes and rotations θ, Φ, ψ , respectively
 e_x and e_y : line-of-sight error coordinates

The platform's half-cone pointing error can be assumed to be 0.1° . The main contributions are due to mechanical errors, thermoelastic distortion errors, and AOCS errors. The total error can then be flowed down into angular errors per axis:

$$\begin{cases} 0.055^\circ \text{ on Roll and Pitch axes} \\ 0.05^\circ \text{ on the Yaw axis} \end{cases} \quad (10)$$

These angular errors are particularly important during the open-loop acquisition phase, while the performance is different during the closed-loop pointing and tracking thanks to the coarse and fine pointing control systems. During this phase, by using a Quadrant

Photodetector (QPD), it is possible to estimate independently the two angular errors in azimuth and elevation, and model the two angles as independent Gaussian random variables [23], which considerably simplifies the tracking loop design. State-of-the-art tracking systems are expected to make only negligible contributions to the pointing error and to perform very close to this Gaussian approximation. Output signals from the QPD are summed and differenced to generate the azimuth and elevation angular deviation estimates. Since the error bias is assumed to be zero, the resulting radial pointing error is therefore Rayleigh-distributed:

$$P(\epsilon) = \frac{\epsilon}{\sigma_\epsilon^2} e^{-\epsilon^2/2\sigma_\epsilon^2} \quad (11)$$

where σ is the rms standard deviation of the probability distribution, assuming radial symmetry, $\sigma = \sigma_x = \sigma_y$ and $\epsilon = \sqrt{\epsilon_x^2 + \epsilon_y^2}$. From Eq. 11, we can calculate the probability of burst error P_E , which occurs when the signal irradiance at the target receiver becomes lower than the threshold required to ensure the average BER. When considered from the pointing and tracking point of view, burst errors occur when the instantaneous pointing loss exceeds the nominal value in the link budget. At a data rate of 100 Mbps and a pointing/tracking system bandwidth of 100 Hz, in the 0.01s before the control system adjusts the pointing error, 1 Megabit of data would be lost! The probability of burst error is given by

$$P_E^* = \int_{\epsilon^*}^{\infty} P(\epsilon) d\epsilon \quad (12)$$

where ϵ^* is the limit pointing error assumed in the link budget. When ϵ exceeds this value, a burst error occurs. Equation 12 yields the relationship between the probability of burst error and the rms standard deviation of the pointing error probability distribution:

$$\epsilon^* = \sigma \sqrt{-2 \ln P_E^*} \quad (13)$$

The magnitude of σ is determined by the dynamics of the host satellite and the operation of the optical system, therefore they are specified here in general terms over a range of representative values. To use these relationships within the link budget, we relate them to the beamwidth needed to close the link and achieve the desired bit error rate.

While up to this point the communication method has not been taken into account, when analysing the link budgets it is intuitive that the spatial tracking error affects the coherent detection channel more severely than direct detection. The advantage of using a heterodyne system for its higher sensitivity is quickly offset by the smaller

gain and the larger power penalty due to pointing error [23]. As a result, for systems with large pointing and tracking errors, the direct detection channel is preferred over the coherent detection channel despite the sensitivity. To fulfill the requirements of thermal control for the payload and solar panel orientation, Galileo satellites follow a dynamic yaw steering law, which is performed continuously, including colinearity phases as described in Section 3.6. Therefore, during nominal operations the AOCS maintains its attitude using its four Reaction Wheels (RW) for attitude control. Due to this continuous motion and to its solar array drive mechanisms used to track the sun, there are error sources onboard the platform. The main hosting requirements on the platform regard pointing knowledge and pointing stability, needed for both link acquisition and tracking [24] [25]. The link budgets were calculated for a nominal pointing error of $5 \mu rad$ as a worst-case scenario, which requires from the platform and terminal values of σ rms error for different values of P_E or link availability:

- $P_E = 1\%$ leads to $\sigma = 1.6 \mu rad$ rms pointing error
- $P_E = 0.1\%$ leads to $\sigma = 1.3 \mu rad$ rms pointing error
- $P_E = 0.01\%$ leads to $\sigma = 1.1 \mu rad$ rms pointing error

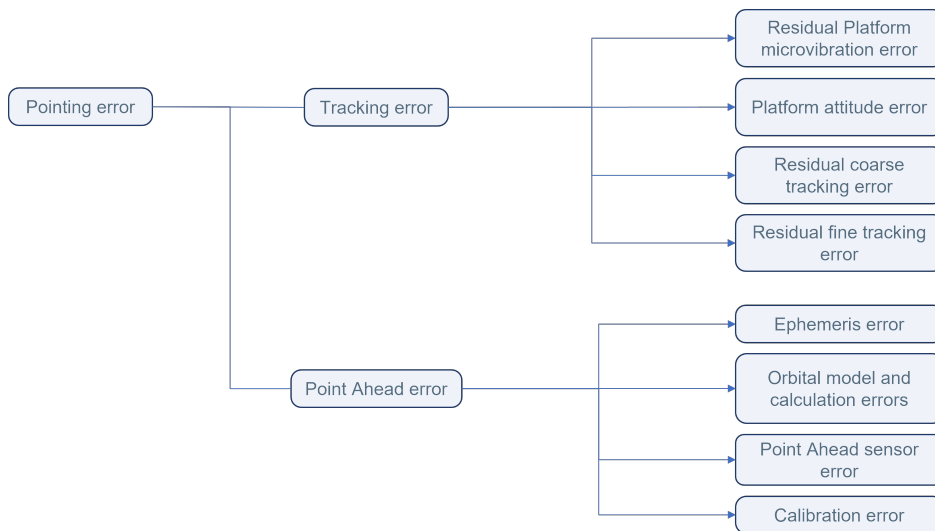


Figure 13: Contributions to the pointing error

Micro-vibrations are low-amplitude vibrations at relatively high frequencies. They are mainly generated by on-board mechanisms and propagate through the satellite

structure towards the LCT or other sensitive equipment. The main sources are reaction wheels and solar array orientation mechanisms [25].

3.8 Receiver

The receiving component, in combination to the modulation scheme used, is an important contribution to the performance of any communication system in terms of achievable link distance and data rate. In this chapter, the different types of detection methods will be discussed and analysed.

3.8.1 Choice of Detection method

FSO communication uses either noncoherent or coherent detection techniques. While non-coherent direct detection models the transmitted light in its corpuscular nature, coherent data transmission uses its representation as an electromagnetic wave. Therefore, it increases the channel's degrees of freedom as it allows the use of modulation formats based on amplitude, frequency, phase and polarization information. In non-coherent detection, the transmitted light is directly received by the photodetector, and individual photons generate electrons in the photodetector, generating the signal and noise currents which are proportional to the number of photons received. In coherent communication, the received light is combined with the one from the LO and they both reach the photodiode. Added complexity is caused by the sensibility to phase modulation, so the ability to recover the in-phase and quadrature components of the signal. In systems with high data rates (> 100 Mbps) or for power limited systems (very long distances), coherent detection is nonetheless generally preferred over direct detection. Coherent detection can then be either homodyne or heterodyne: the basic difference is in the signal carrier and local oscillator frequency. In heterodyne detection, the Local Oscillator frequency is not the same as the signal-carrier frequency, while in homodyne detection the incoming signal is mixed with a Local Oscillator whose frequency and phase are locked with that of the signal carrier waves via a Phase Lock Loop (PLL). Despite being a more complex circuit to implement, it offers higher sensitivity than heterodyne detection. It should be noted that although its ideal performance is better when compared to direct detection methods, there are two main things to keep in mind:

- Advantages in receiver sensitivity can be made irrelevant by signal degradation due mainly to misalignment and pointing error, so the system would often work in non-optimal conditions;

- In a system where very high data rates are not a crucial design driver, direct detection technology should be sufficient to close the link although with higher sensitivity.

These are some of the aspects that make up the trade-off between the two types of detection.

3.8.2 Detectors

Photodetectors can be PIN or APD. A PIN diode is one type of photodetector, used to convert an optical signal into an electric signal. PIN-based receivers are relatively simple and cheap but they are the least sensitive. The main difference with Avalanche Photodiodes (APDs) can improve performance by providing internal gain and an overall 10-dB benefit over PIN-receivers by amplifying the signal during the detection process [26] [27].

3.8.3 Required Received Power

One of the photodetector's main characteristics is the responsivity R_0 , defined as the ratio of current over optical power, measured in Amperes/Watts, The received optical power in the form of photons hitting the detection area and excites the photoelectrons from the semiconductor's valence band via the detector material's responsivity. R_0 depends on signal wavelength $\lambda = c/\nu$ and the semiconductor's quantum efficiency η , which characterizes the light-to-current conversion. The maximum value for R_0 is reached when all photons are converted into electrons, when η of the photodiode is 100%:

$$R_0 = \frac{\eta q}{h\nu} \quad (14)$$

Receiver sensitivity is another important parameter and is related to the lowest power level at which the receiver can detect the optical signal and demodulate its data. Sensitivity is often measured in terms of average received photons per bit (PPB):

$$n_{av} = \frac{\eta P_R}{h\nu R_b} \quad (15)$$

where $h\nu$ is the photon energy at the operating wavelength and R_b is the bit rate or data rate. Sensitivity mainly depends on photon detection technique, modulation format, photodetector, and background noise. This allows for an easier performance comparison of different receivers. In direct detection receivers, thermal noise and shot noise contributions generally dominate [14]. In tables 4 and 3 are the values

for minimum power required at data rate of 1 Gbps for both detection methods and both wavelengths.

	Direct Detection	
	1064 nm	1550 nm
Sensitivity	20 PPB	20 PPB
Minimum P_{req}	4.67 nW = -53 dBm	3.2 nW = -54 dBm

Table 3: Sensitivity (minimum power required) for direct detection

	Coherent Detection	
	1064 nm	1550 nm
Sensitivity	9 PPB	9 PPB
Minimum P_{req}	2.1 nW = -56 dBm	1.44 nW = -58 dBm

Table 4: Sensitivity (minimum power required) for coherent detection

The values found in these tables will be used later in the link budgets.

3.9 Operating Wavelength

The choice of operating wavelength depends upon many factors that include:

- Availability of components
- Required output power
- Background noise power
- Gain vs beamwidth: lower wavelengths are related to higher gain, but smaller beamwidths and thus higher pointing error losses
- Detector sensitivity: the sensitivity of detectors is determined by their detection efficiency, and their availability is limited by the operating wavelength.

The dependence on wavelength of the sensitivity of available receivers must in fact also be considered. Currently, the two primary wavelengths used for free-space optical links are 1550 nm, used by terrestrial optical fiber communications and 1064 nm, based on the Nd:YAG solid state laser technology and used by the EDRS data relay links. The 1064 nm and 1550 nm lasers have been commonly used in many space missions, for their characteristic to be very efficient in respect to the detectors technologies and therefore they are the two technologies considered in this study.

3.10 Point-ahead-angle and Doppler Shift

The signal transmitted is required to be pointed at an angular offset from its relative location so that it effectively hits the receiver at a proper spatial temporal location. This displacement has to be compensated both in position and frequency, after calculating respectively the Point-Ahead Angle and the Doppler Shift between two linked satellites. Both depend upon the relative velocity between the two satellites, and can be accurately achieved with the help of the updated ephemerides data. The primary task is to calculate the motion information (position, speed and acceleration) between pairs of satellites. The positions and velocities of the satellites have been calculated within the Matlab©Satellite Scenario environment. The simulations were run for 6 orbital periods, with the default orbit propagator SGP4 (Simplified General Perturbations-4). The positions and velocities taken from the output are defined in the *Geodetic Celestial Reference Frame (GCRF)*, with the origin at the center of the Earth and orthogonal vectors \mathbf{I} , \mathbf{J} , \mathbf{K} , with the \mathbf{IJ} -plane that is closely aligned with the equator. Then, the relative position and velocity between any two satellites A and B can be obtained by vector operations under the geocentric equatorial inertial coordinate system.

$$\begin{cases} \mathbf{r}_{AB} = \mathbf{r}_{IJK}^A - \mathbf{r}_{IJK}^B \\ \dot{\mathbf{r}}_{AB} = \dot{\mathbf{r}}_{IJK}^A - \dot{\mathbf{r}}_{IJK}^B \end{cases} \quad (16)$$

In Eq. 16, \mathbf{r}_{AB} and $\dot{\mathbf{r}}_{AB}$ are relative positions and velocity of satellite B with respect to satellite A. At last, the point-ahead angle is represented in the coordinate system of the satellite payload and the Doppler shift is calculated with respect to both spacecraft payloads:

$$\theta_{PA} = 2 \frac{|\dot{\mathbf{r}}_{AB} \times \hat{\mathbf{r}}_{AB}|}{c} \quad (17)$$

$$\frac{\Delta f}{f} = - \frac{\dot{\mathbf{r}}_{AB} \cdot \hat{\mathbf{r}}_{AB}}{c} \quad (18)$$

Among all possible links between satellites in the constellation, PAA varies between $26.7 \mu\text{rad}$ and $49 \mu\text{rad}$. Compared to the divergence of beam which is between $10 \mu\text{rad}$ and $20 \mu\text{rad}$ depending on the operating wavelength, one can see how it is important to account for this offset. Values for Doppler shift Δf range between $\pm 3.2 \text{ GHz}$. This effect requires that the Tx laser shall be tunable with a range of at least $\pm 7 \text{ GHz}$, and may require minimum Bandwidth and fast frequency tuning of the optical filter, and/or of the LO when using a coherent receiver [28]. The Doppler shift between satellites in the same orbit is small compared to the shift between satellites in different orbits, which is in turn quite considerable and will have an impact on the signal reception.

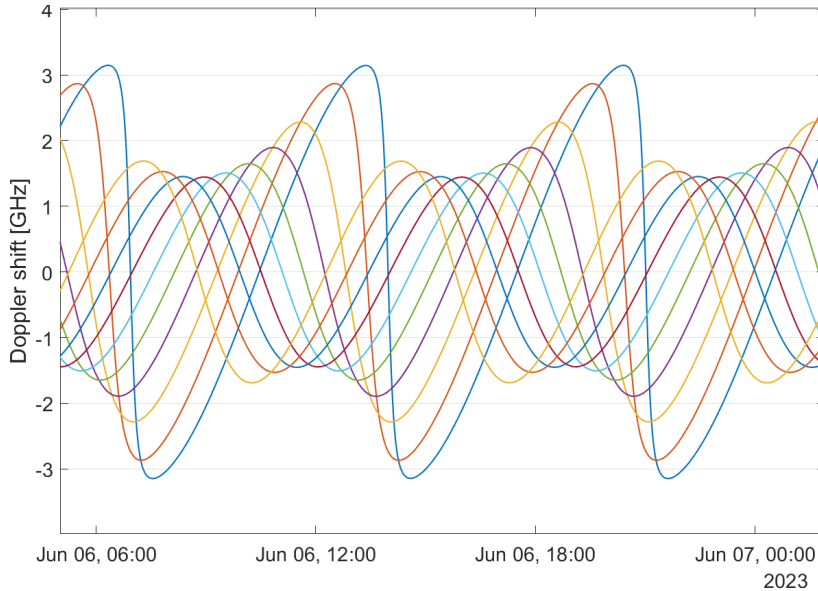


Figure 14: Doppler shift between Satellite ID1 and other satellites from different orbital planes

3.11 Link Budget

The main drivers that impact the ISL link budget are the link range, the signal wavelength and pointing errors. The first two affect the path losses: the longer distances and shorter wavelengths both increase path losses. The values for range among all satellite pairs have been derived from the simulations, excluding opposite satellites of the same orbital plane since these links are never possible. As a first approximation, the telescopes have a circular aperture and the antenna gains G_T , G_R are related to

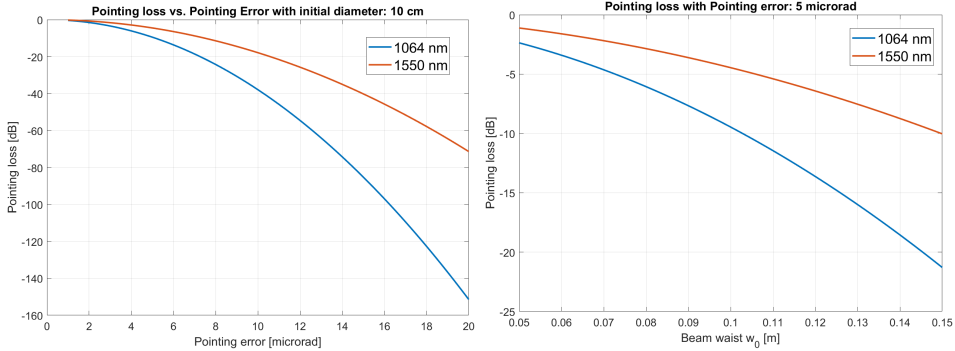
the diameters D_T and D_R according to

$$G_{T,R} = \left(\frac{\pi D_{T,R}}{\lambda} \right)^2 \quad (19)$$

which is applicable in the hypothesis of a diffraction limited laser beam. Substituting this into the link budget equation reveals the $1/\lambda^2$ dependence of the received power P_R . The full-angle beam divergence can then be obtained as

$$\theta = \frac{\lambda}{D_T} \simeq \frac{\lambda}{\pi w_o} \quad (20)$$

The diameter of the transmitting and receiving telescopes were assumed to be 10 cm, which for the two wavelengths yield beamwidths of $13.6 \mu\text{rad}$ and $10.4 \mu\text{rad}$. This yields a beam diameter at intersatellite distances that ranges from 200 to 600 meters for 1064 nm wavelength, and from 280 to 900 meters for 1550 nm wavelength. Having a larger beam radius allows for more margin in pointing errors: pointing loss is one of the main components in signal loss, and degrades quickly with even very small pointing errors. With a 10 cm - diameter telescope and pointing error $\epsilon = 5 \mu\text{rad}$, pointing losses are approximately -4.5 dB .



(a) Pointing loss vs overall pointing error (b) Pointing loss vs Beam Waist with fixed pointing error

By comparing the link budgets for the two operating wavelengths, it is clear that a trade-off must be made between achieving higher gain and reducing signal reception degradation due to pointing error.

Figure 16 shows the laser beam's diameter with distance, where it can be noted that at the minimum link distance the beam diameter is below 200 meters, and at maximum link distance can reach up to 900 meters.

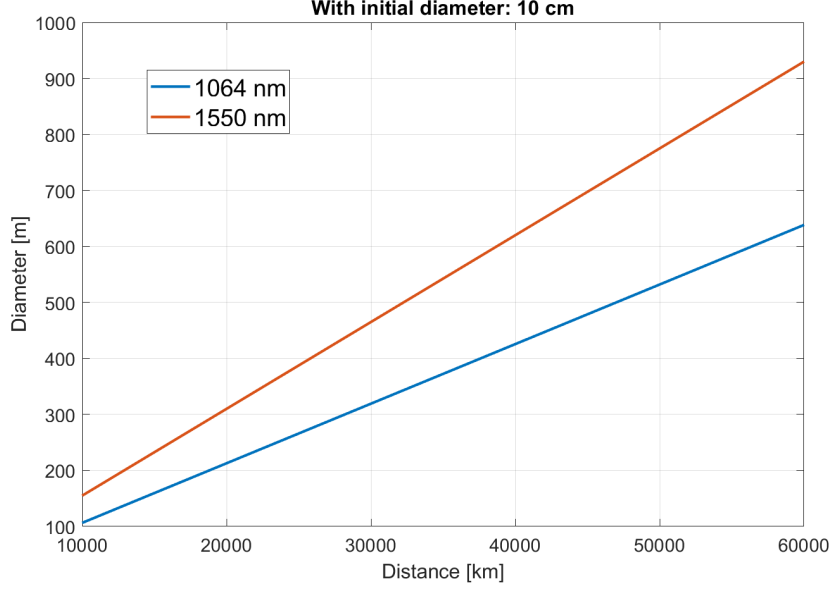


Figure 16: Beam diameter vs Link Distance

Other contributions to the link budget are pointing losses, free space loss, transmitter and receiver optical efficiency, and filter losses. Laser transmission losses are caused by the coupling of the signal with the optical system and its propagation through the telescope. On the receiving side, it is necessary to consider mainly the primary and secondary mirror losses and truncation losses due to the overfilling of the beam into the antenna aperture. Usually, all these non-idealities are considered in the efficiency parameter $\eta_{T,R}$.

$$\begin{cases} L_{pT,R} = e^{-G_{T,R}\theta_{T,R}^2} \\ L_s = \left(\frac{\lambda}{4\pi d}\right)^2 \\ \eta_{T,R} = 0.8 \end{cases} \quad (21)$$

Such that the final equation for received optical power is:

$$P_R = P_T \cdot G_T \cdot G_R \cdot L_{pT} \cdot L_s \cdot \eta_T \cdot \eta_R \cdot G_C \cdot L_{Tx,Rx} \quad (22)$$

In Fig.17 are the curves described by Eq.22 for both the considered wavelengths.

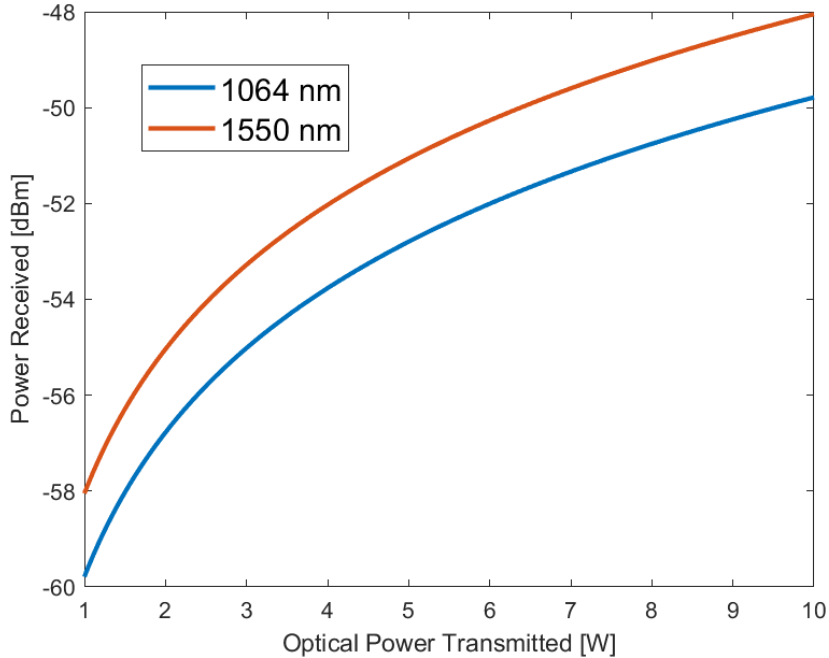


Figure 17: Power received versus optical power in output from the transmitter

If the assumption is taken that the receiver Field-of-View is sufficiently wide, the receiver pointing error has a negligible effect on the receiver signal power. Therefore, the receiver antenna gain depends only on the aperture diameter and wavelength. It has been demonstrated that the BER for a direct detection PPM system depends only on transmitter power, gain and rms pointing error [23]. Pointing and tracking losses are the only random input to the link budget and there are several models taking them into account, of which used here is the Gaussian beam model. Coding schemes are considered as recommended in the OISL standards [12], [13], [29]. Putting together the data from tables 3 and 4 with the preliminary power budget from Fig.17, we can calculate the output power required from the transmitting terminal for the various cases. This power was calculated with the worst case of a $5 \mu\text{rad}$ rms pointing error and a link margin of 3 dB, as per optical communications standard recommendation [12].

Although the narrower beam delivers more power density, this advantage is subsided mainly by misalignment losses. The case in which less power is required is the case for transmission with a wavelength of 1550 nm and coherent detection.

	1064 nm	1550 nm
Gain $P_{T,R}$ with $D_T = 10$ cm	109.4 dB	106.1 dB
Pointing loss with $\epsilon = 5 \mu\text{rad}$	-9.5 dB	-4.5 dB
Free space loss	-296.6 dB	-293.3 dB
Receiver losses	-5 dB	-5 dB
Transmitter losses	-1 dB	-1 dB
Coding (FEC) gain	3.5 dB	3.5 dB
$P_{R_{req}}$, direct detection at BER = 10^{-9}	-53 dBm	-54 dBm
$P_{R_{req}}$, coherent detection at BER = 10^{-9}	-56 dBm	-58 dBm
Optical power $P_{T_{req}}$ required with Direct Detection	9.5 W	5 W
Optical power $P_{T_{req}}$ required with Coherent Detection	4.7 W	2 W

Table 5: Link budgets

CHAPTER 4

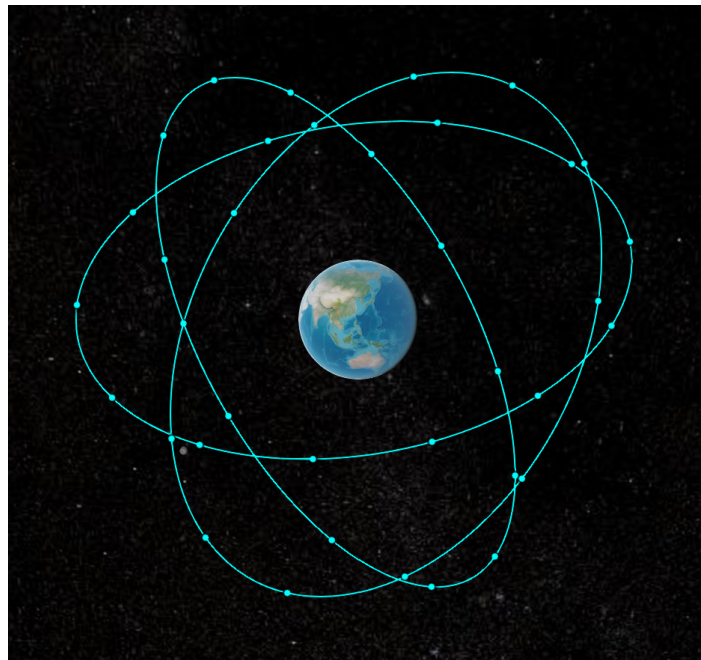
Network Architecture

Connecting the satellites in a constellation by intersatellite links offers a full range of possibilities [30]: besides ranging and time synchronization, ISLs can be used to distribute data and updates for the SVs in a short period of time, as well as improve the constellation's autonomy by depending less on ground station availability. The two basic use cases for Intersatellite Links are data dissemination and intersatellite ranging (ISR). ISR measurements are the pseudo-range measurements between any two satellites via ISL, and they are performed during every link between a pair of satellites. The accuracy of the system is improved with the increasing number of measurements from different satellites, so the optimal goal for ISR is to maximize the number and the spatial diversity of inter-satellite links. Inter-satellite communication, on the other hand, focuses on the volume of transferred data, number of links necessary to reach the target, and communication delay. In terms of frequency of the contacts, the requirements for the two different use cases are different: for communication a lower repointing frequency is preferable, in order to have a stable link to simplify network protocols; for ranging, as we said before, the goal would be to maximize the number of contacts. Based on these requirements, in this chapter the principles of link building are provided.

4.1 Inter-satellite link planning

The analysis is based on a nominal constellation of 36 MEO satellites in a Walker 36/3/1 configuration with an orbital altitude of 29599.8 km, future Galileo FOC constellation as shown in Fig.18. The satellites show a 10-day ground track repetition, so simulations were done by propagating the orbital scenario for 10 days. In Table 6 the orbital elements of the Galileo constellation are reported, published by EUSPA [31].

Semimajor Axis	29599.8 km
Eccentricity	0
Inclination	56°
RAAN	77.632, 197.632, 317.632
Argument of periapsis	0
Period	14.08 h

Table 6: Orbital Parameters**Figure 18:** Galileo FOC constellation

The task is to find a relatively simple rule with which to determine the intersatellite links. To start, a visibility analysis was done on the satellites in the constellation. The scenario was propagated for 10 days, and the access percentages of each satellite-to-satellite contact were calculated. It was found that for each satellite 5 of the 35 possible links were not accessible at some time during the simulation period. According

to this criteria, in the visibility matrix a 1 is assigned to links with 100% visibility over time, while a 0 is assigned to links with $< 100\%$ visibility, as represented in Fig.19. Considering that the relative positions between the satellites repeat every orbital period (~ 14 hours), the links which suffer some earth shadowing are always the same, and 100% visibility also means that the links are permanently available over time. This leaves 30 links available at all times for each satellite, and allows to avoid corrections of the matrix a posteriori due to limited visibility of some satellite-to-satellite contacts. This analysis could also be generalized including the 5 missing links, by restricting their validity to certain time intervals. In this case, all considerations taken would remain the same. The ISL Network is composed of:

- A variable number of **Gateway** (GW) satellites, nodes downloading to ground the telemetry received by other satellites and uploading to them the telecommands received by ground hubs.
- A variable number of **Non-Gateway** satellites, nodes using space-to-space links for receiving/sending data to/from a GW and/or other NGs, but are not connected directly to a ground hub.
- A variable number of Ground Hubs (GHs), which are ground stations used to uplink/downlink data to the satellites via ISL.
- Space to Space Contacts, consisting of either RF or Optical links between satellites
- Ground to Space Contacts, consisting of S-band/C-band links between GHs and GWs
- An ISL Network communication protocol (Network and Physical Layer)

The number and connectivity of these elements can change depending on the availability of space and/or ground infrastructure, system configurations, and planned or unplanned events.

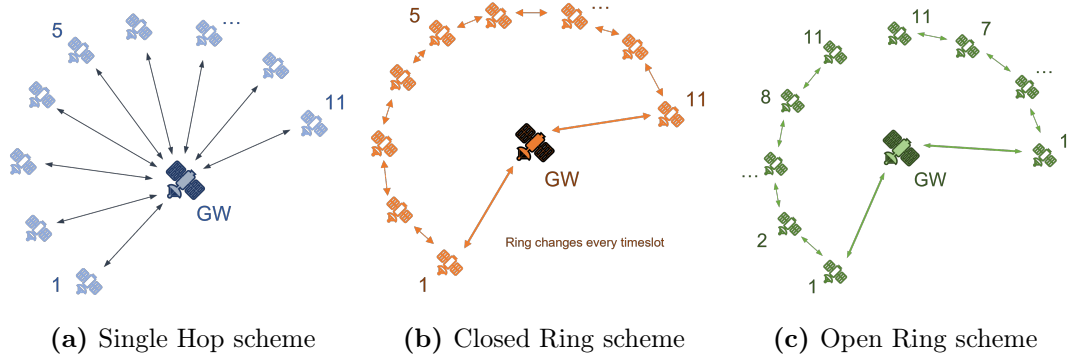
Taking into account this visibility analysis, the task is to find a repeatable method with which to define a contact plan respecting the requirements mentioned previously. Each satellite has at all times 30 possible links with 30 different satellites, and is equipped with two payloads. Therefore, there are 15 possible configurations in which all pairs are contacted with both payloads, and 30 configurations with one payload. A few of these configurations are shown in 20.

Each different scheme resulting from these combinations has different geometric characteristics such as minimum and maximum ranges, and relative azimuth and elevation angles between the satellites. Each satellite embarks two ISL payloads that can operate either simultaneously or at different times.

4.2 OISL system

The first step is the definition of the network layer, in terms of routing schemes and routing logic. Three main ISL routing schemes were considered, all of which consist of the use of two operational ISL payloads per satellite:

- Centralized single-hop: gateways send to the target non-gateway its specific telecommands and moves on to the next contact, while non-gateways send their telemetry to the gateway for downlink. In this case, real-time operations are limited to only happen during GW-NG contacts. Inevitably, in this configuration there are added delays in both the upload of telecommands and the download of telemetry from the constellation. In each timeslot, there are still two links for each satellite, but based on the channel capacity, which links carry data and which links, for example, only perform ranging measurements, depends on the available bandwidth.
- Closed real-time Ring: the data is relayed within the ring from link to link leading from source to destination, relying on both satellite terminals transmitting simultaneously. Any satellite that receives data belonging to another satellite forwards it via the other ISL interface.
- Open real-time Ring: taking advantage of the bidirectional links, this configuration consists of the two payloads relaying the data through each chain, from link to link, reaching each target NG satellite.



4.2.1 Contacts structure

The ISL contacts are executed following pre-defined rules and can be divided in the following main subslots:

- **Repointing of the ISL terminal:** each satellite processes the SSCT and the Clock and Ephemeris data received to compute pointing information. The Orbit and Clock data has a validity of 75h, and must be updated periodically to be able to establish the ISLs.
- **Transmission:** in this subslot the two satellites both:
 - Generate ISR measurements, which are then disseminated through the L-band and/or embedded in the telemetry
 - Exchange TC packets, which can include Orbit and Clock data, SSCT, satellite commands, and Mission data
 - Exchange TM packets, which can include satellite telemetry and ISR measurements

It's interesting to note that about 90% of the time is allocated to repointing, while the rest, 10%, is enough to deliver several Mb of data to 36 satellites. The relative duration of the two subslots are opposite in a scenario with RF links, in which about 70% of the time is occupied by data transmission (35% in one direction and 35% in the other direction) and the other 30% is allocated to repointing and other subslots.

4.2.2 ID Association

The spacecraft IDs are assigned to every satellite with an ID number from 1 to 36. The assignment is chosen such that every 3 S/C IDs, the satellites are on the same

orbital plane:

$$\begin{cases} \text{for } i = 1 : 3 : N_{satellites} - 2 \rightarrow \text{1st orbital plane} \\ \text{for } i = 2 : 3 : N_{satellites} - 1 \rightarrow \text{2nd orbital plane} \\ \text{for } i = 3 : 3 : N_{satellites} \rightarrow \text{3rd orbital plane} \end{cases} \quad (23)$$

In this way, there is a link between the satellite IDs and the geometry of the constellation. The Association Matrix includes the role each satellite has during a specific period, as well as other information.

4.2.3 Timeslot structure

The case of the scenario with dissemination through Real-Time Ring, whether open or closed, was studied more in detail. The timeslot structure could look like the one described in Fig.22:

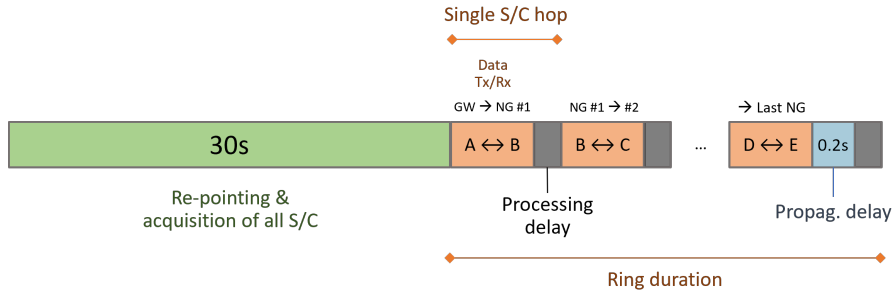


Figure 22: Timeslot structure for a ring scheme from satellite A to satellite E

The first subplot is allocated to repointing, which happens in parallel for all satellites in the constellation and is taken as 30 seconds in a first iteration, assuming data from the state of the art [32]. The smaller orange subslots are dedicated to data transmission from satellite A to satellite B, B to C, and so on until the dissemination scheme’s last NG satellite. Other subslots account for:

- *on-board processing delay* t_{rep} , which is the transfer latency from one ISL link to the second active link, which per requirement is at most 100 ms. To comply with this requirement at the data rate of 50 Mbps, 50 Mbps on-board data transfer is needed, which can easily be met with SpaceWire technology;

- *propagation delay* t_{proc} of 200 ms, which accounts for the time took for the light to have travelled from satellite to satellite and makes sure that the last data packet has reached the target satellite. The value considers the worst-case of maximum distance.
- *queueing delay* t_{queue} is not considered here but it is another potential contribution to the latency of the links, and must be considered in more detailed analyses. It should be noted, however, that bidirectional links with much higher capacity would probably lower this latency contribution with respect to the current RF link performance.

Without other requirements or restrictions, the data transmission subslots can last an arbitrary amount of time, and a first analysis was done assuming the minimum link duration as equal to the signal propagation time, 200 ms. To this minimum value, a margin of $t_{ISR} = 5$ seconds was added in order to account for signal quality during execution of the intersatellite ranging measurements. Therefore, the time-to-disseminate is calculated as:

$$TTD = t_{rep} + t_{proc} * N_{Hops} + t_{ISR} \quad (24)$$

where N_{Hops} is the number of hops needed to reach the target satellite, and depends on the dissemination scheme. The first conservative assumptions taken are: minimum data rate of 50 Mbps at maximum link distance and 30s for repointing time. This time is then plotted for each case:

		i+1	i+2	i+3	i+4	i+5	i+6	i+8	i+9	i+11	i+12	i+13	i+14	i+15	...
1	P1	2	3	4	5	6	7	9	10	12	13	14	15	16	
	P2		36	35	34	2	32	31	29	28	27	26	25	24	23
2	P1	1	4	35	6	2	33	8	10	29	27	14	25	16	23
	P2		3	36	5	1	7	32	30	11	13	26	15	24	17
3	P1	4	1	6	7	8	4	33	11	12	14	15	16	25	18
	P2		2	5	36	4	34	9	31	30	28	27	26	17	24
4	P1	3	2	1	7	8	35	34	12	31	29	16	27	26	25
	P2		5	6	1	3	9	10	13	32	13	15	28	17	18
5	P1	6	7	8	2	1	10	11	13	14	16	17	18	19	20
	P2		4	3	2	9	36	35	6	32	30	29	28	26	26
6	P1	5	8	3	2	1	12	14	33	31	18	30	20	27	
	P2		7	4	9	10	11	36	5	15	17	30	19	28	21
7	P1	8	5	10	3	12	1	15	16	18	19	20	29	22	
	P2		6	9	4	11	2	13	8	34	32	31	30	21	28
8	P1	7	6	5	4	3	2	16	35	33	20	31	30	29	
	P2		9	10	11	12	13	14	7	17	19	32	21	22	23
9	P1	10	11	12	13	14	15	1	18	20	21	22	23	24	
	P2		8	7	6	5	4	3	17	36	34	33	32	31	30
10	P1	9	12	7	14	5	16	2	1	35	22	33	24	31	
	P2		11	8	13	6	15	4	18	19	21	34	23	32	25
11	P1	12	9	14	15	16	5	3	20	22	23	24	33	26	
	P2		10	13	8	7	6	17	19	2	36	35	34	25	32
12	P1	11	10	9	16	7	6	4	3	1	24	35	34	33	
	P2		13	14	15	8	17	18	20	21	23	36	25	26	27

Figure 24: Example of a Contact Plan over time

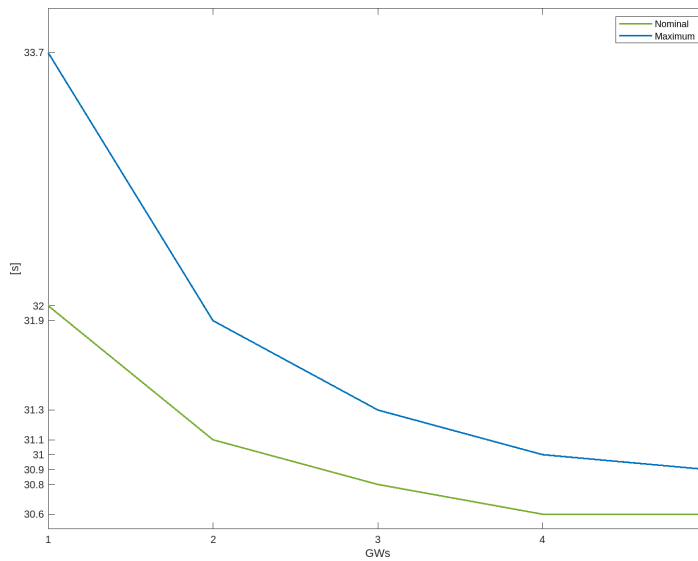


Figure 23: Minimum dissemination time, in the case of a ring configuration scheme and maximum number of hops

Even in the worst case of maximum number of hops, latencies are very low. At each interval, as can be seen from the contact plan, each satellite contacts a new satellite, resulting in maximum ISR measurement diversity. In fact, as the configurations from Fig.20 are executed in sequence, the resulting contact plan is represented as an example in Fig.???. End-to-end latency budgets can then be calculated, and the contributions

for each service to overall latency are reported in tables 7 and 8. After the message is received at the Galileo Sensor Stations and Service Centres, data is forwarded to the Control Centre for the generation of the new navigation message, and then to the TTC for uplink. Taking into account contributions for scheduling and uplink delay of 2 seconds (included in the Uplink contribution), the message is then forwarded from the gateway(s) to the other satellites according to the connectivity matrix. The message is then downlinked directly to the user, from the satellites via L-band. To calculate the components, a few assumptions are taken:

- 36 satellites
- A variable number of GWs, from 1 to 5
- A variable timeslot duration, as defined in Fig. 23
- Open ring scheme and Single Hop Scheme
- Variable number of hops, mainly dependent on the number of GWs

The latency budgets calculated are then used to compare cases for the different schemes.

Message reception and inputs preparation	127 s
Uplink (from 1 to 5 GWs)	712 s, 544 s, 346 s, 249 s, 218 s
Broadcast	101 s
Total with 1 Gateway	940 s = 15.7 min
Total with 2 Gateways	772 s = 12.9 min
Total with 3 Gateways	574 s = 9.6 min
Total with 4 Gateways	477 s = 8 min
Total with 5 Gateways	446 s = 7.4 min

Table 7: Latency Budget for Single Hop

Message reception and inputs preparation	127 s
Uplink (from 1 to 5 GWs)	5.7 s, 3.9 s, 3.3 s, 3 s, 2.9 s
Broadcast	101 s
Total with 1 Gateway	234 s = 3.9 min
Total with 2 Gateways	232 s = 3.9 min
Total with 3 Gateways	231 s = 3.9 min
Total with 4 Gateways	231 s = 3.85 min
Total with 5 Gateways	230.9 s = 3.8 min

Table 8: Latency Budget for Open Ring

It's clear that, since for every hop an entire timeslot has to be added, overall latency is much higher compared to an Open Ring scheme where it remains more or less the same, around 4 minutes. In this case, the contribution for uplink is not even dependent on the repointing time, since the initial repointing can simply be included in the first 127 seconds as it would be happening simultaneously. In the first case, on the other hand, as repointing time increases, overall latency grows.

4.2.4 Connectivity Matrix

The Connectivity Matrix (CM) is then formed by the ID pairs representing each connection taking place. Two CMs are generated, one per satellite payload. An example can be seen in Fig.25, which corresponds to the link topology in Fig. 27.

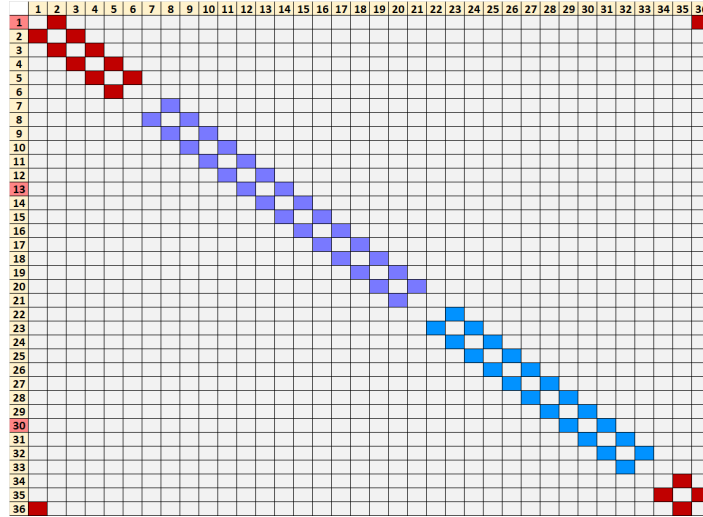


Figure 25: Example of a Connectivity Matrix

4.3 Hybrid RF and Optical system

The second type of system which was investigated is an architecture with a hybrid communication system, with both RF and optical capabilities. The system presents two different types of payload: a Ka-band antenna (one operative + one redundant) and two optical terminals (two operative + one redundant). This system would have a few unique characteristics, and would enable interesting new use cases:

- Full decoupling of the communication and ranging functions, using the two technologies' different advantages: the communication is done through the optical high-data rate channel, while ranging is done through the ka-band antenna with fast repointing and large beamwidth
- Permanent connections become possible, among satellites in the same orbital plane or on different planes
- Real-time access to the constellation, data dissemination without constraints given by ranging measurements
- Precise ODTs with ranging measurements done by the RF antenna

As we saw in previous chapters, there are certain requirements between communication and ranging capabilities that produce design conflicts within the inter-satellite link

network. This architecture was mainly investigated as a transition system between the two technologies, and kept in consideration for future studies. ISL geometries in which the links are permanent would have several benefits, first of all in having a constant connectivity matrix, while the association matrix would only need to be updated to take into account GW visibility to ground. The network topology in this case is constructed following two different logics for the different links: the optical communication links can be decoupled from for ISR measurements requirements, and can therefore be permanent. For this reason, they are designed starting from the visibility matrix and from the configurations found for every different offset defined, some of which were shown in 20.

For each of these schemes, we can calculate the range of distances between the satellites and the angular velocity of the terminal. In case of standing connections with permanent links and in a nominal scenario, there would be no reason to repoint or change the topology of the network. For this reason, the most convenient scheme should be chosen from the ones found. Following for example the criteria for minimum link distance, the two most interesting schemes are:

- 3 intra-plane rings:
 - Fixed distances at ~ 18000 km
 - time to disseminate is in the order of a few seconds
 - Each GW is connected to the satellites in its orbital plane with its two payloads
- A single inter-plane ring connecting all satellites
 - Mean distance of ~ 30000 km: as shown in ??, ranges go from a minimum of 15000 km to a maximum of 45000 km
 - Terminals rotate at 2 deg/minute, negligible w.r.t. yaw steering counter-rotation
 - time to disseminate is in the order of a few seconds
 - One GW would be enough to contact the whole constellation

Although there is no requirement for being able to use one single Gateway and reduce the workload on the Ground Segment, the latter scheme is also interesting for different use cases. Another advantage in the use of both configurations is that in case of failure of one or more terminals, each satellite can easily repoint to the next one and still be able to close the link.

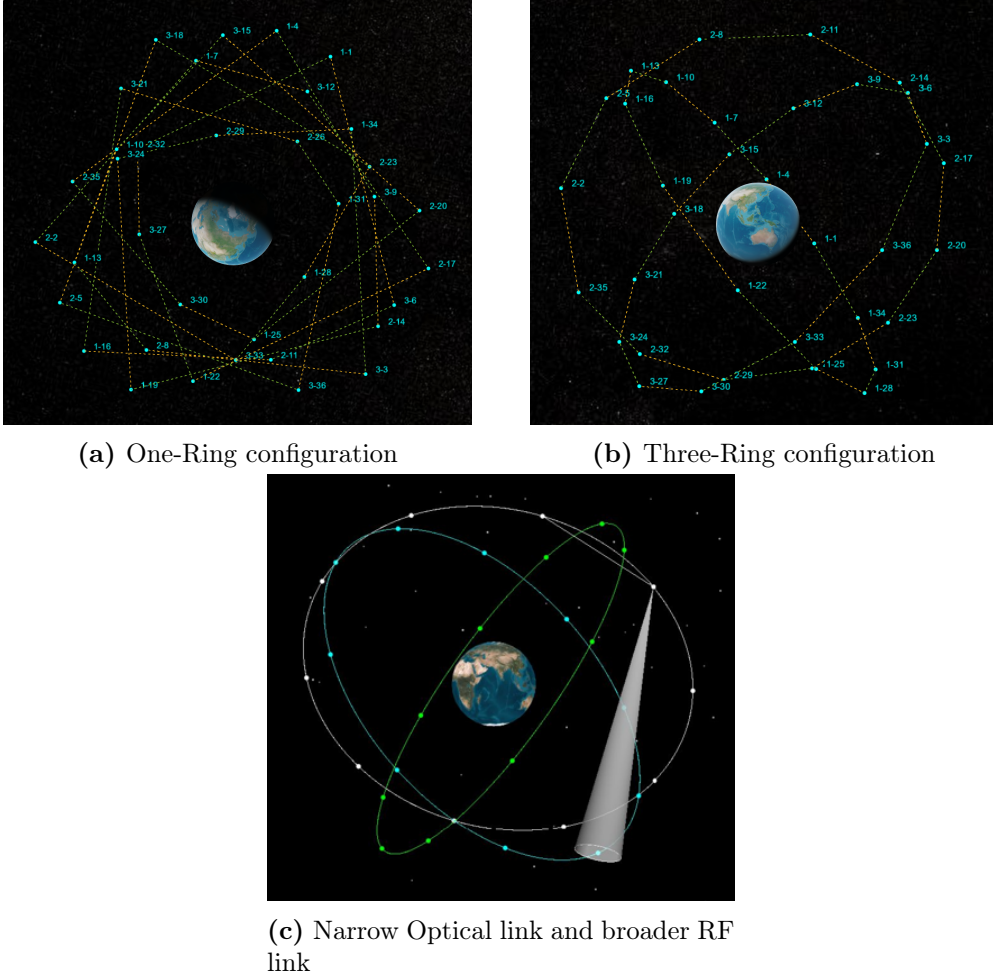


Figure 26: Possible network topologies for a hybrid network architecture, and view of the different links coexisting in the constellation

In Figures 26a and 26b are represented the two schemes considered for the hybrid architecture. The main difference between the two architectures is the orientation of the links and the inter-connectivity among the satellites in the constellation: in 26a, the links are all inter-plane and all satellites are connected in a single chain, while in 26b the links are all intra-plane and the three rings are separate, or independent, from each other. The RF antenna, on the other hand, is repointing frequently in order to obtain its ISR measurements.

4.4 Operational Use Cases

The main groups for use cases can be categorized as Mission Data dissemination, Inter-satellite Ranging and Monitoring & Control:

- Lower-volume real-time data with very short latency (< 1 minute) which does not need to reach the whole constellation;
- Mid-volume data with target latency of < 20 minutes which does not need to reach the whole constellation;
- High-volume data flows with a long refresh period, therefore latency can be < 4 hours;
- ISL Ranging (ISR) measurements: the ISR data is used by the Ground Segment to improve the ODTS and therefore the quality of the service to the users;
- Satellite commanding and monitoring: send batch of commands with/without CEV, to a single sat/whole constellation, live execution, interlocked; download telemetry and events from single sat/whole constellation;

The system generates and uploads mission data with a specific periodicity. It then generates all contact schedules so to make sure that all mission data is uploaded via ISL in compliance with the required latency. Apart from nominal processes, the ISL network also allows ground operations to quickly identify anomalies and react to satellite failures.

With respect to Data Dissemination, there are some parameters that identify the network performance:

- The end-to-end latency, i.e. the time it takes for messages to be sent from ground, through the ISL network, and back to ground through the L-band navigation signal;
- The time to disseminate, so the time it takes from the Gateway (or Gateways) to transmit the data to all the Non-Gateways, also dependent on the number of hops necessary from the first satellite to the last (depending on the type of data, the number of Gateways and the network topology).

Based on the number of Gateways, a different number of configurations for data dissemination are possible. In Fig.27 an example is shown for a 3-gateway configuration,

in which, according to the ring geometry, each gateway has a certain number of satellites on its "path" until it encounters the next gateway. This path is followed for data dissemination, so that each payload forwards data for only a smaller subset of satellites. In this example, satellites with ID number 1, 13 and 30 were arbitrarily chosen as gateways (the number preceding the ID with a "-" stands for its orbital plane, so all satellites belong to either orbital plane 1, 2 or 3). Gateway 1 communicates to satellites with ID numbers 2 up to 6 with one payload, and to satellites with ID numbers 36 down to 34 with the second payload. Satellite 13 communicates with ID numbers 14 up to 21 with one payload, and to satellites 12 down to 7 with the second payload. Finally, satellite 30 communicates with ID numbers 31 up to 35 with one payload, and to satellites 29 down to 22 with the second payload. The dissemination method can be repeated for any number and any choice of gateway satellites.

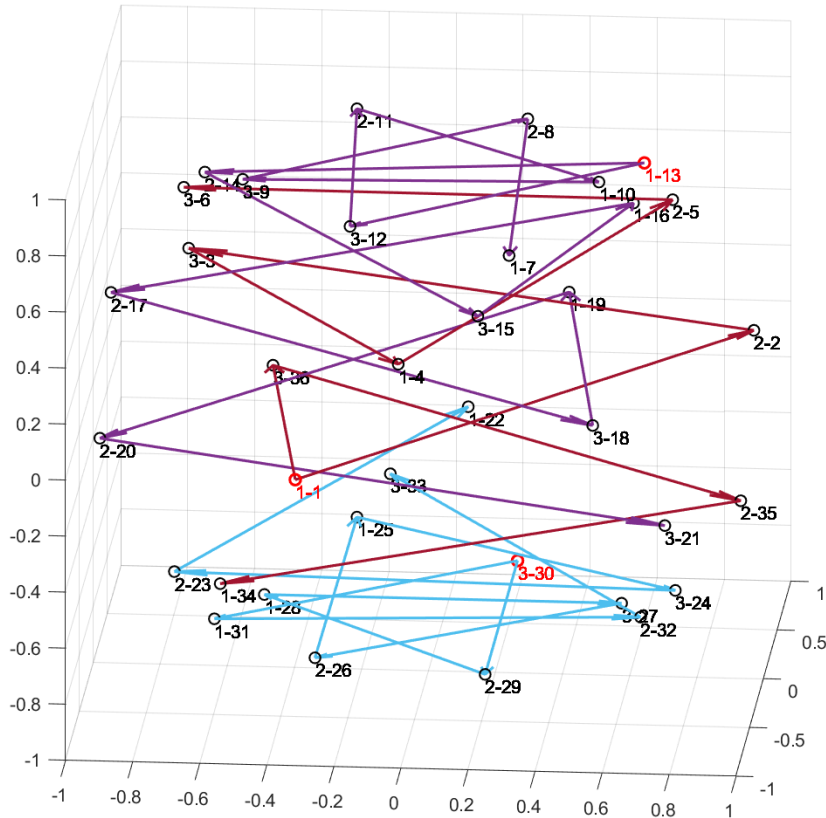


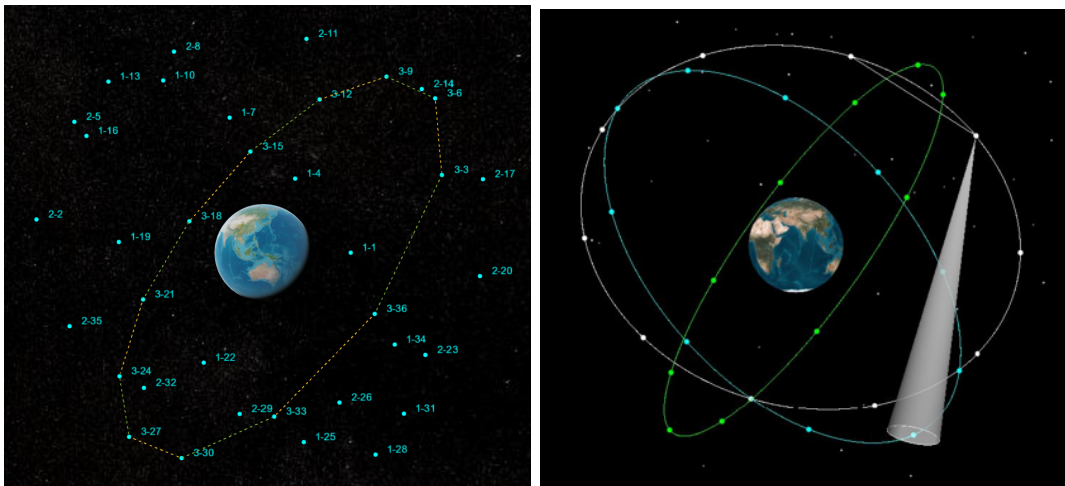
Figure 27: Example for a dissemination path with 3 Gateways, each communicating with two operative payloads. This representation in normalized 3-D space was used to take into account more information than was obtainable in a MATLAB Satellite Scenario, and represents the gateway satellites in red, and their separate "rings" or "branches" in three different colors

Putting together use cases and network architectures, we can make the best use of each topology with respect to each use case. Any volume of data flow can be handled by an optical channel. In the case of a hybrid system however, there is the question of whether the RF link also serves the function of communication or only transmission of ranging information. The Ka-band links would be characterized with a data rate 100 times smaller than the optical links, and could therefore be used either for low-volume low-latency data or for high-volume high-latency data. Their potential use also depends on how many antennas it is possible to mount on the satellite platform (a real time ring, for example, is not possible with only one operational payload). From the point of view of the ISR use case, a hybrid system would enable a simpler decoupling of this function with respect to the communication function. In this case,

the Ka-band antenna would be in charge of doing frequent repointing and generate the ranging measurements. In an OISL system on the other hand, the frequency of the measurements depends on the performances of the terminal. Performances similar to the current system can be achieved, but the comparison would not be fair as most likely a re-design of the concept would be required, since the baseline technology and the overall system would be completely different.

4.5 Transition System

Between a future system where all satellites will be equipped with one technology, there should be a system in which different generations of satellites coexist, and must work together. One possible way to implement this would be to have the new generations of satellites, equipped with laser terminals, launched in positions where they are always in visibility among themselves. The new generation of satellites would also be equipped with RF technologies as an interface to the previous generation. In this way, taking advantage of the optical high-data rate links, keeping the satellites connected could lead to having a distributed Gateway in orbit, so as to add more flexibility to dissemination within the constellation, reduce latencies, increase space segment reliability and reduce dependence on the ground segment. The satellites with RF communication payloads, on the other hand, would still operate as usual but with easier access to a Gateway, facilitating data dissemination and possibly contact planning.



(a) Transition system with one orbital plane equipped with LCTs (b) Hybrid system with both Optical and RF links

CHAPTER 5

New Use Cases for GNSS

5.1 Towards routine contacts with ISL

From tables 7 and 8 we can see that a higher-capacity channel enables the transmission of bigger volumes of data in very short amounts of time, and this opens to more possibilities than what can be defined with an RF network with limited capacity. For each satellite, the number of frames in uplink dedicated to routine contacts can be estimated to be around 20000, including mainly telecommands and mission data, with a certain margin for other services.

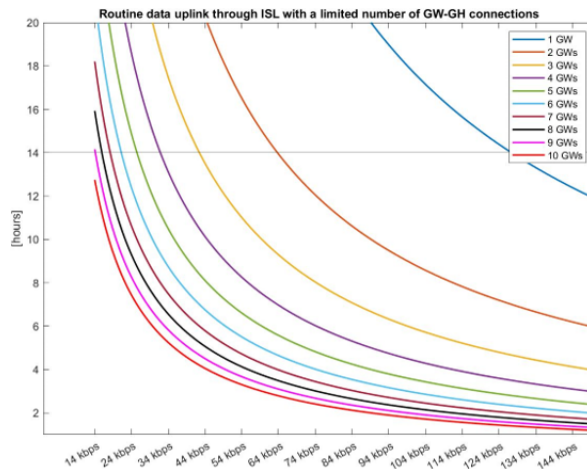


Figure 29: Time necessary for dissemination vs Data Rate, for different number of gateways connected to ground

To uplink all necessary transfer frames for every satellite, so in the most demanding scenario, calculations were done for a data volume of 720000 TFs, as in Fig.29. The figure shows the uplink's Data Rate versus time required to send all data, and each curve represents data uplink done by n gateways and corresponding n ground hubs.

Without ISL, routine TT&C S-band contacts last a minimum of 60 minutes, with a frequency of once every orbit (~ 14 hours). To move routine TT&C contacts to the ISL network, a certain number of ground-space links are required. The upload of all data, in all cases, is guaranteed within one orbit as can be seen from the 14-hour limit drawn in Fig.29. All the transfer frames make up about 6.4 Gb of data uploaded to the constellation. The time taken to uplink is approximately $\frac{6.4 \text{ Gb}}{DR_{S\text{-band}} * GW_s}$, so it depends on the S-band data rate and the number of simultaneous uplinks.

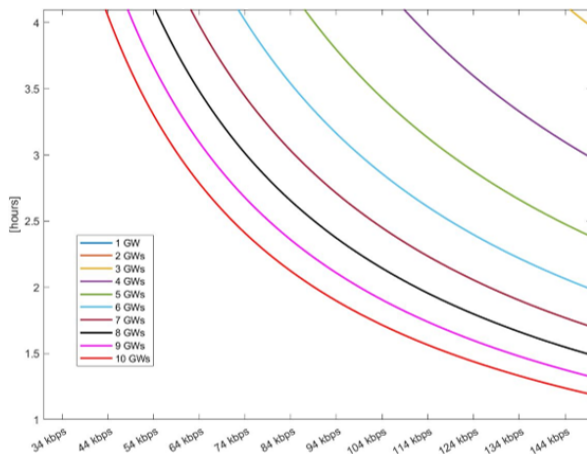


Figure 30: Time necessary for dissemination vs Data Rate, zoom on 4-hour limit

From Fig.30, we can notice that with more than just 3 Gateways, it is possible to update all 36 satellites with their 20000 transfer frames every 4 hours circa. To cope with the S-band bottleneck, a data rate of ~ 148 kbps is needed to upload all data within 4 hours. To avoid a future ground-to-space bottleneck, solutions like GEO-relay and ground-to-space optical links can be investigated, as mentioned in the next sections.

5.2 European Data Relay System

The EDRS (European Data Relay System) provides optical and microwave data relay services between LEO satellites and the ground through geostationary (GEO) satellite nodes. In order to cope with an S-band bottleneck, the services offered by the EDRS nodes could be useful as relay with ground. Users may choose to receive the data at their own ground stations in order to have direct access to it [33]. The two nodes EDRS-A and EDRS-B were launched respectively in 2016 and 2019, with 15 years of

operative life: this use case can be considered until the years 2031-2034, which is quite limiting for Galileo. The link range between the Galileo satellites goes from 7000 km to 62000 km, with minimum visibility over one period of 92%. The range for EDRS links has a maximum of 45000 km at the nominal data rate of 1.8 Gbps. With the payload on the nadir face of the platform, satellites that are within the 45000 km range and have the EDRS satellites in their hemispherical FoR can link to the nodes and use them for data relay. This also enables new use cases which require having high capacity space-to-ground links, although posing a constraint on the link's modulation scheme and wavelength.

However, the transmitting and receiving modulation scheme for the EDRS nodes is BPSK at 1064 nm wavelength, therefore posing a significant constraint on the communication system. These specifications at the moment are also not compliant with optical communication standards issued by the CCSDS and the SDA.

5.3 Ground - Space Optical Links

The **European Optical Nucleus Network** or ONN is an initiative between European space agencies and industrial partners to overcome current limiting factors for OGS technology. Its core elements are:

- Multiple stations connected to a single point of contact
- Ground Stations design based on the use of COTS components, for cost effectiveness
- Capacity for remote and automated operation
- Multi-site network but with common technological standards

Quote: With the proven advancement of optical ground station technology and laser communication space terminals in Europe, and with the advent of common standards on optical communications, we have reached the ideal conditions to trigger a concrete first use case and it is expected that with such a champion, we may soon enter the era of optical communication [34]. The initial Nucleus Network consists of optical ground stations from ESA in Tenerife, Spain, DLR in Almeria, Spain and Kongsberg Satellite Services (KSAT) in Nemea, Greece. All stations have been connected to the KSAT operations centre in Norway. The Network should go into full bloom in 2023, and aims to add other ground stations across the globe.

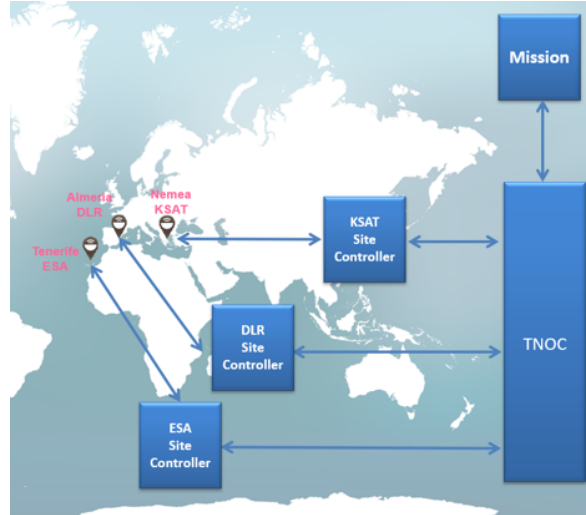


Figure 31: Initial Optical Nucleus Network

The logic behind the Network is to increase the spatial diversity of optical ground stations around the globe so to reach high availability percentages for Ground Station Access to acceptable levels.

In a ground-to-space link, the link budget also needs to take into account atmospheric effects and losses. The two main sources for this phenomenon are Mie scattering and geometrical scattering, which can be used to model attenuation in the atmosphere. Received power then has an additional factor of L_A , atmospheric loss [35].

5.4 ODTS

There is currently no uniform standard for evaluating the "goodness" of inter-satellite measurement [36] [37] [38] [39] [40] [41], so the theory of satellite positioning can be used as reference: when pseudo-range data is used for real-time applications, the DOP (Dilution of Precision) values are the measure for the geometrical strength of the observation model. It only depends on the observable configuration and observation time of the local satellites. The effect of geometry is characterized by the parameters known as the GDOP and the PDOP, which are respectively the Geometric DOP and the Position DOP. These two parameters are often used as a criterion for selecting optimal visible satellites to improve the positioning accuracy by using intersatellite measurements and to evaluate the performance of the links [42] [43] [44] [9]. The PDOP value corresponding to a number of established links between satellites can be

calculated to reflect the quality of the geometric configuration of ISR measurements. If x, y, z are the transmitting satellite's coordinates, τ is the satellite's clock offset and c is the speed of light. Then one can define the PDOP as:

$$PDOP = \frac{\sqrt{[Var(x) + Var(y) + Var(z)]}}{URE} \quad (25)$$

where $Var(\cdot)$ denotes the variance of a random variable [45]. If (x_i, y_i, z_i) is the position of the i th satellite when the signal is sent, then one can write the sets of equations as

$$R_i = r_i - c\tau = \sqrt{[(x_i - x)^2 + (y_i - y)^2 + (z_i - z)^2]} - c\tau \quad (26)$$

where r_i is the range and R_i is the pseudorange of the i th satellite from the transmitting satellite. The method was used to justify the restriction of 35 links to 30 (with 100% visibility), and the results yield a mean PDOP which is higher of about 0.1, still under the value of 2. It was then also used to verify the difference between the two permanent standing-connection configurations described in section 4.3. The method in this case is slightly modified, with an added fixed matrix H_{fixed} representing the virtually continuous measurements taken by the permanent links. Also in this case, results weren't very different among the two cases.

The criteria of link establishment must be studied through different methods in order to plans connections that are valuable for orbit determination purposes. Finding a subset of measurements which produces the same quality in this sense would be beneficial for the communication and data dissemination system, increasing reliability and reducing the complexity of space network protocols.

5.5 Novel architectures for GNSS

An architecture as that proposed in 5 with such an advanced network connectivity can enable new opportunities and can be exploited from many different sides. For a GNSS constellation, reliable synchronization across the elements of the constellation in a quasi-inertial frame is essential to obtain a precise navigation solution for users. During nominal operation, all the elements of the constellation share the measured offsets between the frequency references, relayed in a very short time via OISLs. Continuous ISL connects all satellites and enables direct synchronization of the satellites at a level not achievable today [46], [44]. The pseudorange ρ^k associated with satellite k is defined by:

$$\rho^k = c(t_R - t_T^2) = \|\vec{r} - \vec{r}^k\| + c(\delta - \delta^k) + \dots + \eta^k \quad (27)$$

with t_k denoting the time of transmission by satellite k measured using the satellite's clock, and with t_R denoting the time of reception measured using the receiver's clock. δ and δ^k are the clock offsets of the different clock used at the transmitter and receiver. \vec{r}^k is the satellite's position, and η^k is the additive white Gaussian noise. The dots represent delays and biases which are not of much interest in this paper.

As one can see from Eq.27, ρ^k depends on the clock offsets, but not on absolute time. Thus, as proposed in [47], it is natural to consider the possibility of directly synchronizing the satellites' transmissions. This would require not clocks in the proper sense, but oscillators onboard the satellites for generating the signals that remain stable during the synchronization process [47].

Permanent links within a constellation can also be the basis for a completely different approach to satellite navigation with a relativistic navigation system, as in the concept of a Relativistic Positioning System (RPS). An advantage of this architecture is that the system of satellites can be autonomous and constitutes a primary reference system, with no need to define a terrestrial reference frame [48].

With the generalization of concepts like the one in [47], some of its advantages can be adjusted for a system similar to the hybrid system proposed in this thesis, with permanent optical links and a freely schedulable link. These considerations are mainly two: without a LEO backbone the MEO satellites can relay the signals among each other, for time transfer and real-time data dissemination; the inter-satellite ranging can be done by the RF payload on board the satellites, which represents the freely schedulable link.

CHAPTER 6

Conclusions and further developments

The conclusions are not black or white in favor of one or the other ISL technology. Many things regarding the enabling technology should be assessed before coming to a more definitive conclusion, especially regarding the acquisition scheme performance and the ODTS enhancements brought by higher precision in ISR measurements. The most favorable system seems to be the hybrid architecture for the satellite communication system, which takes into consideration both technologies' pros and cons, and has a real possibility of bringing different enhancements to the system. To increase the efficiency of an only-OISL system, one thing which must be improved is the understanding of the impact of ISR measurements on the ODTS process. This work is based on the current concept for ODTS with ISLs for Galileo, but also mentioned are several studies and ideas for future developments that would shape the system with optical inter-satellite links in the following iterations. Further work on the topic can be done by studying more efficient ways to route data decentralizing the single hop scheme, distributing the data also from non-gateway to non-gateway in a way that does not require the satellites to be intelligent but only following the updated connectivity matrices.

References

- [1] S. Chan, “Architectures for a space-based information network with shared on-orbit processing,” 2005. [Online]. Available: <https://api.semanticscholar.org/CorpusID:39610075>.
- [2] B. Eissfeller, T. Zink, R. Wolf, *et al.*, “Autonomous satellite state determination by use of two-directional links,” *International Journal of Satellite Communications*, vol. 18, no. 4-5, pp. 325–346, 2000. DOI: [https://doi.org/10.1002/1099-1247\(200007/10\)18:4/5<325::AID-SAT680>3.0.CO;2-8](https://doi.org/10.1002/1099-1247(200007/10)18:4/5<325::AID-SAT680>3.0.CO;2-8). eprint: <https://onlinelibrary.wiley.com/doi/pdf/10.1002/1099-1247%28200007/10%2918%3A4/5%3C325%3A%3AAID-SAT680%3E3.0.CO%3B2-8>. [Online]. Available: <https://onlinelibrary.wiley.com/doi/abs/10.1002/1099-1247%28200007/10%2918%3A4/5%3C325%3A%3AAID-SAT680%3E3.0.CO%3B2-8>.
- [3] L. ZHAO, X. HU, C. TANG, *et al.*, “Inter-satellite link augmented beidou-3 orbit determination for precise point positioning,” *Chinese Journal of Aeronautics*, vol. 35, no. 4, pp. 332–343, 2022, ISSN: 1000-9361. DOI: <https://doi.org/10.1016/j.cja.2021.05.002>. [Online]. Available: <https://www.sciencedirect.com/science/article/pii/S1000936121001618>.
- [4] X. Ren, Y. Yang, J. Zhu, and T. Xu, “Orbit determination of the next-generation beidou satellites with intersatellite link measurements and a priori orbit constraints,” *Advances in Space Research*, vol. 60, no. 10, pp. 2155–2165, 2017, ISSN: 0273-1177. DOI: <https://doi.org/10.1016/j.asr.2017.08.024>. [Online]. Available: <https://www.sciencedirect.com/science/article/pii/S0273117717306191>.
- [5] C. Wang, Q. Zhao, J. Guo, J. Liu, and G. Chen, “The contribution of intersatellite links to bds-3 orbit determination: Model refinement and comparisons,” *NAVIGATION*, vol. 66, no. 1, pp. 71–82, 2019. DOI: <https://doi.org/10.1002/navi.295>. eprint: <https://onlinelibrary.wiley.com/doi/pdf/10.1002/navi.295>. [Online]. Available: <https://onlinelibrary.wiley.com/doi/abs/10.1002/navi.295>.
- [6] Y. Yang, Y. Yang, X. Hu, *et al.*, “Inter-satellite link enhanced orbit determination for beidou-3,” *Journal of Navigation*, vol. 73, pp. 1–16, Jun. 2019. DOI: [10.1017/S0373463319000523](https://doi.org/10.1017/S0373463319000523).

- [7] K. Maine, P. Anderson, and F. Bayuk, “Communication architecture for gps iii,” in *2004 IEEE Aerospace Conference Proceedings (IEEE Cat. No.04TH8720)*, vol. 3, 2004, 1539 Vol.3. DOI: 10.1109/AERO.2004.1367927.
- [8] J. Xie, H. Wang, P. Li, and Y. Meng, *Satellite Navigation Systems and Technologies*. Jan. 2021, ISBN: 978-981-15-4862-8. DOI: 10.1007/978-981-15-4863-5.
- [9] T. Kur, T. Liwosz, and M. Kalarus, “The application of inter-satellite links connectivity schemes in various satellite navigation systems for orbit and clock corrections determination: Simulation study,” *Acta Geodaetica et Geophysica*, vol. 56, Oct. 2020. DOI: 10.1007/s40328-020-00322-4.
- [10] *ESA - Galileo Second Generation*, https://www.esa.int/ESA_Multimedia/Images/2021/05/Galileo_Second_Generation, Published: 2021-05-27.
- [11] H. Hemmati, *Near-Earth Laser Communication*, eng, 2nd ed. CRC Press, 2020, ISBN: 9780429186721. DOI: <https://doi.org/10.1201/9780429186721>.
- [12] SDA, *Optical communications terminal (oct) standard version 3.1.0*, Washington, D.C., Mar. 2023.
- [13] CCSDS, *Optical communications coding and synchronization*, Washington, D.C., Aug. 2019.
- [14] D. O. Caplan, “Laser communication transmitter and receiver design,” in *Free-Space Laser Communications: Principles and Advances*. New York, NY: Springer New York, 2008, pp. 109–246, ISBN: 978-0-387-28677-8. DOI: 10.1007/978-0-387-28677-8_4. [Online]. Available: https://doi.org/10.1007/978-0-387-28677-8_4.
- [15] R. Lange and B. Smutny, “Homodyne BPSK-based optical inter-satellite communication links,” in *Free-Space Laser Communication Technologies XIX and Atmospheric Propagation of Electromagnetic Waves*, S. Mecherle and O. Korotkova, Eds., International Society for Optics and Photonics, vol. 6457, SPIE, 2007, p. 645 703. DOI: 10.1117/12.698646. [Online]. Available: <https://doi.org/10.1117/12.698646>.
- [16] CCSDS, *Optical communications physical layer*, Washington, D.C., Aug. 2019.
- [17] J. Meng, T. Wei, Y. Wang, *et al.*, “Two-stage frequency compensation for doppler shift on bpsk transceiver with ldpc codes for free-space optical communication systems,” *Frontiers in Physics*, vol. 11, 2023, ISSN: 2296-424X. DOI: 10.3389/fphy.2023.1099867. [Online]. Available: <https://www.frontiersin.org/articles/10.3389/fphy.2023.1099867>.

- [18] M. Guelman, A. Kogan, A. Kazarian, A. Livne, M. Orenstein, and H. Michalik, “Acquisition and pointing control for inter-satellite laser communications,” *Aerospace and Electronic Systems, IEEE Transactions on*, vol. 40, pp. 1239–1248, Nov. 2004. DOI: 10.1109/TAES.2004.1386877.
- [19] Y. Kaymak, R. Rojas-Cessa, J. Feng, N. Ansari, M. Zhou, and T. Zhang, “A survey on acquisition, tracking, and pointing mechanisms for mobile free-space optical communications,” *IEEE Communications Surveys & Tutorials*, vol. 20, no. 2, pp. 1104–1123, 2018. DOI: 10.1109/COMST.2018.2804323.
- [20] E.-H.-E.-0. W. Group, *Esa pointing error engineering handbook*. [Online]. Available: <http://peet.estec.esa.int/handbook/>.
- [21] U. Sterr, M. Gregory, and F. Heine, “Beaconless acquisition for isl and sgl, summary of 3 years operation in space and on ground,” in *2011 International Conference on Space Optical Systems and Applications (ICSOS)*, 2011, pp. 38–43. DOI: 10.1109/ICSOS.2011.5783704.
- [22] R. Lange and B. Smutny, “Homodyne BPSK-based optical inter-satellite communication links,” in *Free-Space Laser Communication Technologies XIX and Atmospheric Propagation of Electromagnetic Waves*, S. Mecherle and O. Korotkova, Eds., International Society for Optics and Photonics, vol. 6457, SPIE, 2007, p. 645 703. DOI: 10.1117/12.698646. [Online]. Available: <https://doi.org/10.1117/12.698646>.
- [23] C.-C. Chen and C. Gardner, “Impact of random pointing and tracking errors on the design of coherent and incoherent optical intersatellite communication links,” *IEEE Transactions on Communications*, vol. 37, no. 3, pp. 252–260, 1989. DOI: 10.1109/26.20099.
- [24] D. Poncet, S. Glynn, and F. Heine, “Hosting the first EDRS payload,” in *International Conference on Space Optics — ICSO 2014*, Z. Sodnik, B. Cugny, and N. Karafolas, Eds., International Society for Optics and Photonics, vol. 10563, SPIE, 2017, p. 105630D. DOI: 10.1117/12.2304091. [Online]. Available: <https://doi.org/10.1117/12.2304091>.
- [25] D. Calzolaio, F. Curreli, J. Duncan, A. Moorhouse, G. Perez, and S. Voegt, “Edrs-c – the second node of the european data relay system is in orbit,” *Acta Astronautica*, vol. 177, pp. 537–544, 2020, ISSN: 0094-5765. DOI: <https://doi.org/10.1016/j.actaastro.2020.07.043>. [Online]. Available: <https://www.sciencedirect.com/science/article/pii/S0094576520304707>.

- [26] D. Caplan, “Laser communication transmitter and receiver design,” *Journal of Optical and Fiber Communications Reports*, vol. 4, pp. 225–362, Sep. 2007. DOI: 10.1007/s10297-006-0079-z.
- [27] D. Giggenbach, “Free-space optical data receivers with avalanche detectors for satellite downlinks regarding background light,” *Sensors*, vol. 22, no. 18, 2022, ISSN: 1424-8220. DOI: 10.3390/s22186773. [Online]. Available: <https://www.mdpi.com/1424-8220/22/18/6773>.
- [28] S. Schaefer, M. Gregory, and W. Rosenkranz, “Investigation of coherent receiver designs in high-speed optical inter-satellite links using digital signal processing,” in *Society of Photo-Optical Instrumentation Engineers (SPIE) Conference Series*, ser. Society of Photo-Optical Instrumentation Engineers (SPIE) Conference Series, vol. 10562, Sep. 2017, 1056251, p. 1056 251. DOI: 10.1117/12.2296112.
- [29] C. NASA, *Coding and modulation for the optical channel*. [Online]. Available: <https://cwe.ccsds.org/sls/docs/SLS-CandS/Meeting%20Public%20Materials/2008/200810.BerlinInput/NASA.Fall108-CCSDS%20optical.pdf>.
- [30] H. Zech, P. Biller, F. Heine, and M. Motzigemba, “Optical intersatellite links for navigation constellations,” in *International Conference on Space Optics ICSO 2018*, Z. Sodnik, N. Karafolas, and B. Cugny, Eds., ser. Society of Photo-Optical Instrumentation Engineers (SPIE) Conference Series, vol. 11180, Jul. 2019, 111800Z, 111800Z. DOI: 10.1117/12.2535954.
- [31] *EUSPA - Galileo*, <https://www.euspa.europa.eu/european-space/galileo/programme>, Updated: 2022-10-18.
- [32] H. Zech, P. Biller, F. Heine, and M. Motzigemba, “Optical intersatellite links for navigation constellations,” in *International Conference on Space Optics — ICSO 2018*, Z. Sodnik, N. Karafolas, and B. Cugny, Eds., International Society for Optics and Photonics, vol. 11180, SPIE, 2019, 111800Z. DOI: 10.1117/12.2535954. [Online]. Available: <https://doi.org/10.1117/12.2535954>.
- [33] ESA, *European data relay satellite system (edrs) overview*. [Online]. Available: <https://connectivity.esa.int/european-data-relay-satellite-system-edrs-overview>.
- [34] E. ESOC, *The european optical nucleus network*. [Online]. Available: <https://esoc.esa.int/content/european-optical-nucleus-network#:~:text=With%20the%20proven%20advancement%20of, champion%2C%20we%20may%20soon%20enter.>

- [35] J. Liang, A. U. Chaudhry, E. Erdogan, and H. Yanikomeroğlu, “Link budget analysis for free-space optical satellite networks,” in *2022 IEEE 23rd International Symposium on a World of Wireless, Mobile and Multimedia Networks (WoW-MoM)*, 2022, pp. 471–476. DOI: 10.1109/WoWMoM54355.2022.00073.
- [36] C. Tang, X. Hu, S. Zhou, *et al.*, “Initial results of centralized autonomous orbit determination of the new-generation bds satellites with inter-satellite link measurements,” *Journal of Geodesy*, vol. 92, Jan. 2018. DOI: 10.1007/s00190-018-1113-7.
- [37] X. Gong, “Parameter integration filter and parameter decomposition filter for autonomous navigation of bds,” *GPS Solutions*, vol. 21, pp. 1–12, Jul. 2017. DOI: 10.1007/s10291-017-0640-7.
- [38] J. Yan, L. Xing, P. Wang, L. Sun, and Y.-W. Chen, “A scheduling strategy to inter-satellite links assignment in gnss,” *Advances in Space Research*, vol. 67, Sep. 2020. DOI: 10.1016/j.asr.2020.09.023.
- [39] P. D’Angelo, T. Guardabrazo, and F. Amarillo, “On-board orbit and clock determination based on cross-link observables: Ranging and time transfer provision system,” in *2012 6th ESA Workshop on Satellite Navigation Technologies (Navitec 2012) & European Workshop on GNSS Signals and Signal Processing*, 2012, pp. 1–8. DOI: 10.1109/NAVITEC.2012.6423114.
- [40] P. D’Angelo, A. Fernández, T. Guardabrazo, and F. Amarillo, “Enhancement of gnss navigation function by the use of inter-satellite links,” Dec. 2012, pp. 1–6, ISBN: 978-1-4673-2010-8. DOI: 10.1109/NAVITEC.2012.6423113.
- [41] P. D’Angelo, T. Guardabrazo, and F. Amarillo, “On-board orbit and clock determination based on cross-link observables: Ranging and time transfer provision system,” Dec. 2012, pp. 1–8, ISBN: 978-1-4673-2010-8. DOI: 10.1109/NAVITEC.2012.6423114.
- [42] C. Liu, F. Zhang, H. Ma, S. Chen, X. Wang, and X. Ye, *Open Astronomy*, vol. 31, no. 1, pp. 348–356, 2022. DOI: doi : 10 . 1515 / astro - 2022 - 0199. [Online]. Available: <https://doi.org/10.1515/astro-2022-0199>.
- [43] S. Han, Q. Gui, G. Li, and Y. Du, “Minimum of pdop and its applications in inter-satellite links (isl) establishment of walker-delta constellation,” *Advances in Space Research*, vol. 54, no. 4, pp. 726–733, 2014, ISSN: 0273-1177. DOI: <https://doi.org/10.1016/j.asr.2014.04.020>. [Online]. Available: <https://www.sciencedirect.com/science/article/pii/S0273117714002683>.

- [44] A. Nardin, J. A. Fraire, and F. Dovic, “Contact plan design for gnss constellations: A case study with optical intersatellite links,” *IEEE Transactions on Aerospace and Electronic Systems*, vol. 58, no. 3, pp. 1981–1995, 2022. DOI: 10.1109/TAES.2021.3135025.
- [45] A. H. PHILLIPS, “Geometrical determination of pdop,” *NAVIGATION*, vol. 31, no. 4, pp. 329–337, 1984. DOI: <https://doi.org/10.1002/j.2161-4296.1984.tb00883.x>. eprint: <https://onlinelibrary.wiley.com/doi/pdf/10.1002/j.2161-4296.1984.tb00883.x>. [Online]. Available: <https://onlinelibrary.wiley.com/doi/abs/10.1002/j.2161-4296.1984.tb00883.x>.
- [46] G. Giorgi, T. Schmidt, C. Trainotti, *et al.*, “Advanced technologies for satellite navigation and geodesy,” *Advances in Space Research*, vol. 64, no. 6, pp. 1256–1273, 2019, ISSN: 0273-1177. DOI: <https://doi.org/10.1016/j.asr.2019.06.010>. [Online]. Available: <https://www.sciencedirect.com/science/article/pii/S0273117719304260>.
- [47] C. Günther, “Kepler - satellite navigation without clocks and ground infrastructure,” in *31st International Technical Meeting of the Satellite Division of the Institute of Navigation, ION GNSS+ 2018*, Sep. 2018, pp. 849–856. [Online]. Available: <https://elib.dlr.de/126622/>.
- [48] G. A., H. M., and U. Kostic, *Relativistic gnss. esa-pecs final report*, European Space Agency, 2014.